Allocation of Ambipolar Charges on an Organic Diradical with a Vinylene-Phenylenediyne Bridge

Journal:	*The Journal of Physical Chemistry Letters*
Manuscript ID	jz-2021-01565r.R2
Manuscript Type:	Letter
Date Submitted by the Author:	18-Jun-2021
Complete List of Authors:	Mayorga-Burrezo, Paula; Institut de Ciència de Materials de Barcelona, Consejo Superior de Investigacions Científicas Bejarano, Francesc; Universitari de Bellaterra, Institut de Ciència de Materials de Barcelona (CSIC) Calbo, Joaquín; Universidad de Valencia, Instituto de Ciencia Molecular Zhao, Xiaotao; Durham University, chemistry De Sousa, J. Alejandro; Universitari de Bellaterra, Institut de Ciència de Materials de Barcelona (CSIC) Lloveras, Vega; Consejo Superior de Investigacions Científicas (CSIC), Institut de Ciència de Materials de Barcelona ICMAB CSIC Bryce, Martin; Durham University, Chemistry Ortí, Enrique; Universitat de Valencia, Instituto de Ciencia Molecular Veciana, Jaume; Universitari de Bellaterra, Institut de Ciència Materials de Barcelona (CSIC) Rovira, Concepció; Consejo Superior de Investigacions Científicas (CSIC), Institut de Ciència de Materials de Barcelona Crivillers, Núria; Universitari de Bellaterra, Institut de Ciència de Materials de Barcelona (CSIC)

Allocation of Ambipolar Charges on an Organic Diradical with a Vinylene-Phenylenediyne Bridge

Paula Mayorga-Burrezo,[†] Francesc Bejarano,[†] Joaquín Calbo,[§] Xiaotao Zhao,[¶] J. Alejandro de Sousa,[†+] Vega Lloveras,[†] Martin R. Bryce,[¶] Enrique Ortí,[§] Jaume Veciana,[*†] Concepció Rovira,[*†] Núria Crivillers[*†]*

[†]Institut de Ciència de Materials de Barcelona, ICMAB-CSIC, Campus UAB, 08193 Bellaterra, Spain

[§]Instituto de Ciencia Molecular, Universidad de Valencia, Catedrático José Beltrán, 2, 46980 Paterna, Spain

[¶]Chemistry Department, Durham University, Durham DH1 3LE, U.K.

[+]Laboratorio de Electroquímica, Departamento de Química, Facultad de Ciencias, Universidad de los Andes, 5101 Mérida, Venezuela.

Corresponding Author

E-mail addresses: ncrivillers@icmab.es, cun@icmab.es, vecianaj@icmab.es, enrique.orti@uv.es

ABSTRACT: Two redox and magnetically active perchlorotriphenylmethyl (•PTM) radical units have been connected as end-capping groups to a bis(phenylene)diyne chain through vinylene linkers. Negative and positive charged species have been generated, and the influence of the bridge on their stabilization is discussed. Partial reduction of the electron-withdrawing •PTM radicals results in a class-II mixed-valence system with the negative charge located on the terminal PTM units, proving the efficiency of the conjugated chain for the electron transport between the two terminal sites. Counterintuitively, the oxidation process does not occur along the electron-rich bridge but on the vinylene units. The •PTM radicals play a key role in the stabilization of the cationic species, promoting the generation of quinoidal ring segments.

TOC GRAPHIC

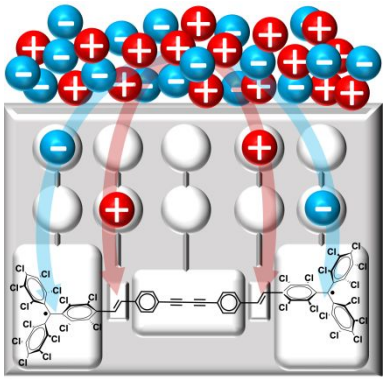

KEYWORDS Oligoyne • PTM radical • Stilbene analogue • Radical anion • Mixed-valence species • Oxidation • Dimerization

To progress in the new era of molecular-scale devices, the understanding of electron transport (ET) phenomena and its relationship with the molecular structure is a compulsory focal point of research. With this aim, for the synthesis of molecular wires,[1,2] connecting two electroactive moieties acting as electron donors (D) or acceptors (A) through molecular bridges is one of the most widely explored strategies to study ET processes. Towards the optimization of the charge transport across the wire, in terms of efficiency and speed, a big effort has been put in the incorporation of different π-conjugated oligomers such as oligo-phenylenevinylene,[3] oligo-thienylenevinylene,[4] oligoynes/polyynes,[5,6] and oligo-fluorenevinylenes,[7] among others, as spacers in D−A conjugates. With these D−A conjugates having easily accessible first redox states, the generation of charge defects, either hole or electrons, is effortlessly achieved, yielding systems with ET phenomena. Particular attention has been devoted to wires bearing identical terminal electroactive species at different redox states, *i.e.*, mixed-valence (MV) systems,[8] which are now considered one of the most straightforward ways to address the ET phenomena owing to the excellent results obtained and the evident synthetic advantages.

More complex phenomena such as ambipolarity can also be pursued following this approach. For instance, two main methodologies are considered for the generation of positive charges: (i)

incorporating donor units or (ii) incorporating an electron-rich bridge where oxidation occurs. Thus, in the event of an electron-rich bridge connecting two electron-withdrawing species, the resulting A−D−A triad can be investigated as an ambipolar structure for the analysis of hole and electron transport.[9] In this regard, perchlorotriphenylmethyl (PTM) radicals are appealing paramagnetic and electroactive carbon-based units, from which carbanionic or carbocationic species can be generated.[10–12] The stabilizing role of the PTM radical in positively charged derivatives has already been reported for A−D−A triads with thienylenevinylene bridges of variable length, and it was explained by the generation of a favorable closed-shell quinoidal structure, resulting from the electron pairing between the lone electron of the PTM moiety and the unpaired electron of the newly formed radical cation species.[13]

In this work, with the aim of exploring fully carbon-based wires and achieving an ambipolar character, a bis(phenylene)diyne bridge end-capped with two PTM radicals (**2-R**, **Scheme 1**) was designed and synthesized. **2-R** is composed by two identical stilbene analogues $[(C_6Cl_5)_2C(C_6Cl_4)$**−C=C−**$Ph-C{\equiv}C-]_2$, in which one of the phenyl rings (that from the PTM moiety) is chlorinated. The −C≡C− bridging bonds were chosen to: *i)* give some rigidity to the structure and *ii)* facilitate the electron transfer across the organic backbone due to an enhanced

electronic coupling,[14,15] similar to carbon-bridged oligo-*p*-phenylenevinylenes (COPVs).[16] Beyond the molecular wire function, it is worth mentioning that diradicals[17] and diradicaloid molecules[18] are of great interest for the understanding of fundamental spin-spin interactions and for potential uses in electronics, spintronics, and batteries. The experimental and theoretical studies presented here point to the formation of positive charges on the vinylene units of **2-R** that are stabilized by the unpaired electron of the PTM radicals. In addition, a mixed-valence system results from the introduction of a negative charge into the PTM.

The synthesis of the target diradical (**2-R** in **Scheme 1**) started from compound **1-H**.[19] First, **2-H** was obtained by the coupling of terminal acetylenes in **1-H** with catalytic Cu(I).[20] Two different routes (a and b in **Scheme 1**) were followed to obtain **2H**, achieving an excellent reaction yield of up to 92% with route b. **2-R** was then prepared almost quantitatively (91%) by deprotonating **2-H** to its corresponding dicarbanion and a subsequent oxidation (see Section 3 of the SI for further details).[21,4] This is an innovative approach to obtain stable oligoyne wires, with the hydrogenated PTM (PTM-αH) moieties acting as bulky heads end-capping the resulting bridge. The same strategy was intended for longer polyynes bridges, attaining the hydrogenated PTM derivatives with 3 and 4 contiguous acetylenes (hexatriyne and octatetrayne, respectively) (Section 3.c, SI).

Unfortunately, low yields and remaining impurities, very difficult to eliminate, were obtained for the corresponding radicals, preventing us to have a broader family to study. **1-R** (**Scheme 1**) was also synthesized to facilitate the analysis of the results obtained for **2-R**.[19]

Scheme 1. Synthetic approach to **1-R** and **2-R**.

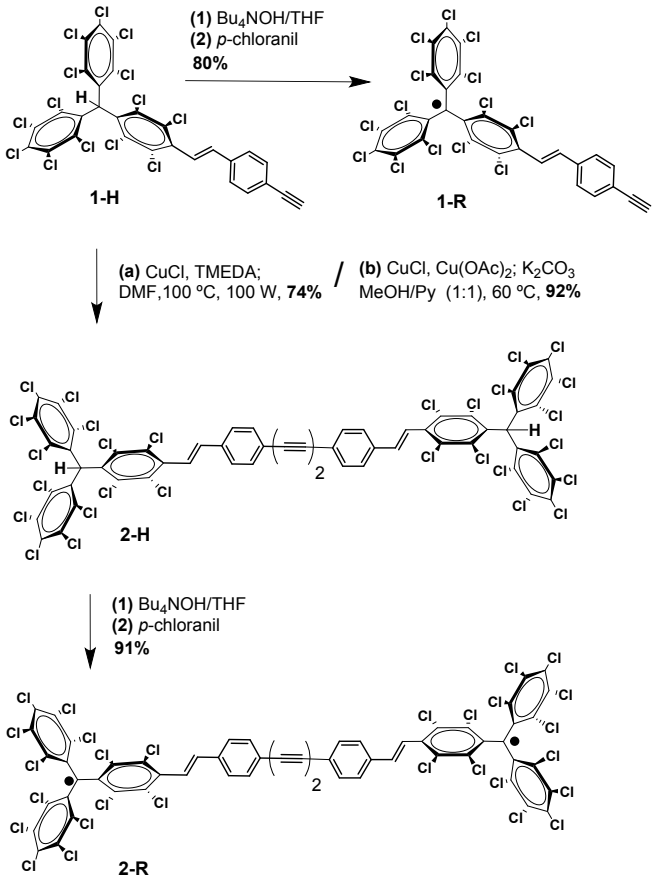

The magnetic and electrochemical properties of **2-R** are depicted in **Figure 1**. The ESR spectrum shows three main overlapped lines centered at g = 2.0028, associated with the coupling of the

unpaired electrons with two equivalent protons (α_H = 0.9 G). Weak satellite lines attributed to the hyperfine couplings with the naturally abundant ^{13}C nuclei of the •PTM cores ($a(^{13}C_\alpha)$ = 15.0 G, $a(^{13}C_{Ar})$ = 4.8 and 6.9 G) were also observed. As expected, all ^{1}H and ^{13}C couplings are half the values showed by the monoradical **1-R** (*i.e.*, g = 2.0026, $a(^{1}H_a)$ = 1.9 G, $a(^{13}C_\alpha)$ = 29.4 G, $a(^{13}C_{Ar})$ = 12.6, 14.3 G).[19] This fact is indicative of a magnetic coupling (J) between the two spins of **2-R** fulfilling the condition $|J|>>|a_i|$, in line with that reported for previous •PTM-based diradicals with different bridges.[21,4]

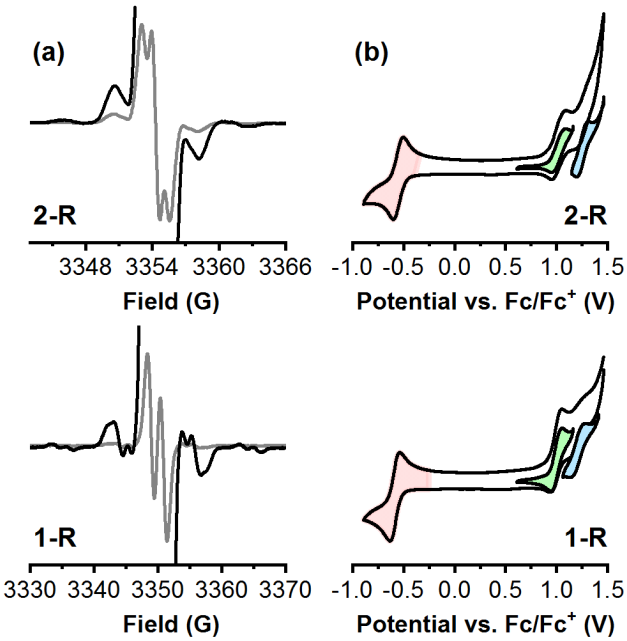

Figure 1. (a) ESR spectra of **2-R** and **1-R** in DCM at room temperature, obtained at normal (grey) and higher gain (black) acquisition conditions. (b) Cyclic voltammogram of **2-R** and **1-R** recorded

at room temperature in 10^{-4} M DCM solutions with 0.2 M TBA-PF_6. CVs at higher positive voltages (in blue and green) were recorded within narrow voltage ranges to clearly observe the waves associated to each oxidation process.

Nearly identical cyclic voltammograms (CVs), with three separated redox processes at almost identical potentials, were recorded for **2-R** and **1-R** (**Figure 1b**). The reversible reduction process ($E^{1/2}$ = –0.55 and –0.58 V *vs* Fc/Fc$^+$ for **2-R** and **1-R**, respectively) was assigned to the generation of the PTM anion form.[22–24] The bielectronic nature of this peak in **2-R** was attributed to a weak electron coupling between the two redox centers through the π-conjugated spacer. Two quasi-overlapped oxidation processes were observed at positive voltages and fully distinguished by CV experiments acquired at limited voltage ranges. The peak at $E^{1/2}$ = 1.26 V (1.22 V for **1-R**) was attributed to the formation of the carbocation of •PTM.[25] The peak at $E^{1/2}$ = 1.02 V in **2-R** was initially assigned to the generation of a positive charge defect, either a cation radical or a dication, on the electron-rich bis(phenylene)diyne bridge. However, two additional independent experimental observations (*i* and *ii*) did not support this hypothesis. Observation *i:* the same peak was detected in the CV of **1-R** ($E^{1/2}$ = 1.00 V) and of the homologous bis(pentachlorophenyl)[4-(4-bromophenyl-*β*-styryl)-2,3,5,6-tetrachlorophenyl]methyl radical (**1-R-Br**)[26] ($E^{1/2}$ = 0. 99 V,

Figure S1), whose chemical structure is identical to **1-R** but with a bromine atom replacing the terminal alkyne group (**Scheme S3**). Therefore, the resulting cation was thought to be necessarily related to the oxidation of the vinylene unit. Although, neither CV nor dynamic pulse voltammetry allowed for a proper charge estimation, similar redox wave areas were found when both oxidation processes were recorded individually. Thus, two bielectronic oxidation processes were assumed for **2-R** considering its •PTM:vinylene (2:2) ratio. Observation *ii:* an irreversible oxidation process at 1.3 V (*vs* Fc/Fc^+) was found for **2-H** (**Figure S2**), whose electroactive response can be exclusively associated to the bis(phenylene)diyne bridge. This last observation suggests that the positively charged species generated on the vinylene unit of the stilbene is only stabilized if the vicinal PTM moiety is in its open-shell form.

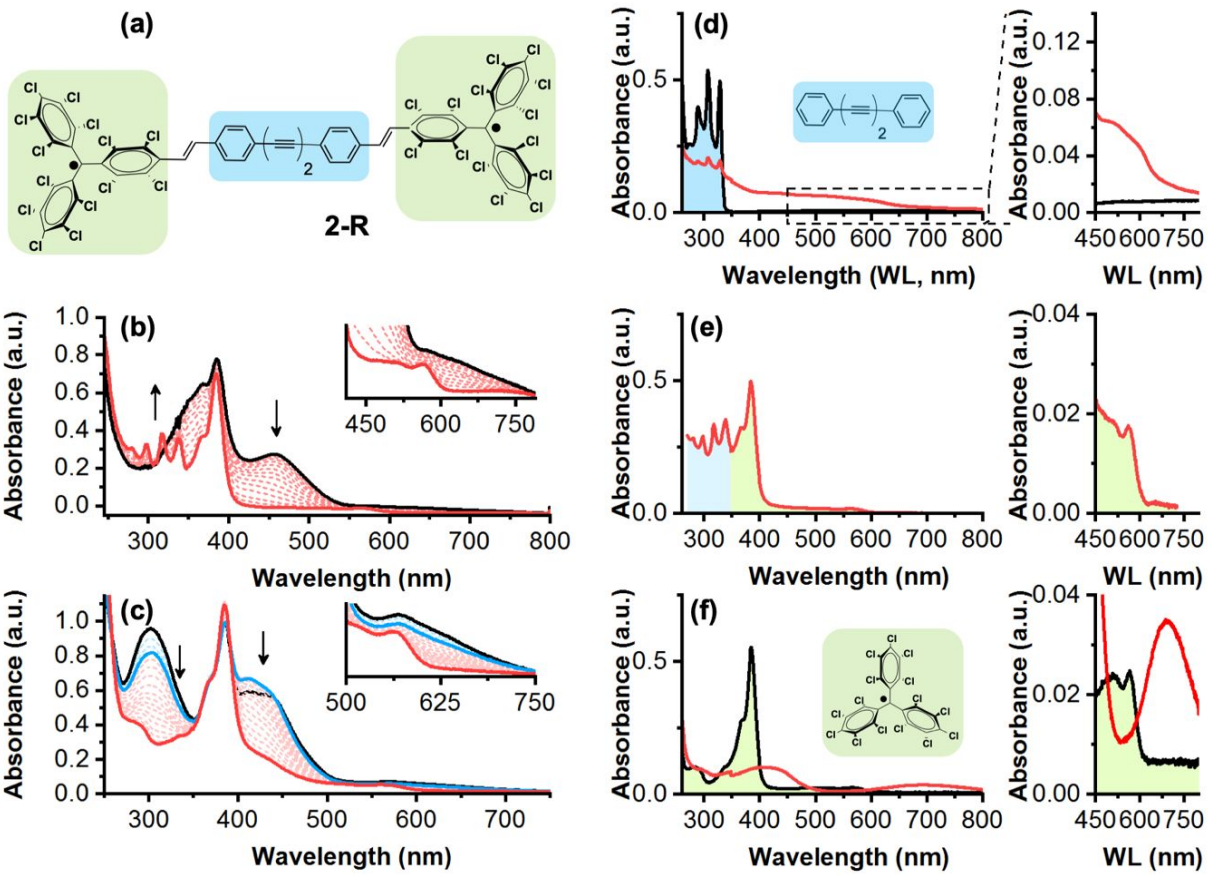

Figure 2. (a) Chemical structure of **2-R**, with colored •PTM (green) and bis(phenylene)diyne (blue) units. UV-Vis electronic absorption spectra of **2-R** (b) and **1-R** (c) obtained during their potentiostatic oxidation (10^{-4} M/ 0.2 M $TBAPF_6$/DCM). Inset: Evolution of the lowest-energy band with the applied positive potential. Black solid line: neutral species. Blue solid line: intermediate species. Red solid line: cationic species. (d)-(f) Comparative UV-Vis electronic absorption spectra of neutral (black) and oxidized (red) species of 1,4-diphenylbutadiyne (d), **2-R**-

Ox (e), and •PTM (f). Shadowed areas following the color scheme in (a) have been included as an eye-guide to identify the contributions of the (d) and (f) spectra into the spectrum of **2-R-Ox**.

Additional UV-Vis electronic absorption and ESR spectroscopic studies were carried out for a deeper analysis of the charged species derived from **2-R**. Based on temperature-dependent ESR experiments, a class-II mixed-valence (MV) radical-anion system was demonstrated upon a partial reduction of the system, according to previous studies of PTM•−bridge−•PTM diradicals[27,28] (Section 5, SI). The generation of the positively charged species appearing at $E^{1/2}$ = 1.02 (*vs* Fc/Fc$^+$) in **2-R** (**2-R-Ox**) was electrochemically addressed and *in-situ* monitored by UV-Vis electronic absorption spectroscopy. The oxidation of electron-rich bridges, such as the bis(phenylene)diyne, usually involves a red-shift of their associated absorption bands derived from the delocalization of the π-electrons behind the charge stabilization, as observed for **2-H (Figure S7)**. Nevertheless, in agreement with the electrochemical data shown above, a totally different behavior was found for **2-R**. The UV-Vis spectrum of **2-R (Figure 2b)** presents two main features at 385 and 450 nm, corresponding to the •PTM chromophores and their conjugation with the bis(phenylene)diyne bridge, respectively. Remarkably, during its potentiostatic oxidation, several narrow features appear at higher energy (~280–340 nm) after the complete vanishing of the broad

band at 450 nm. Similar results were found for **1-R-Ox (Figure 2c)**, whose UV-Vis spectrum shows a vanishing of the conjugation band, whereas the band associated to •PTM remained almost unaltered. Additional spectroelectrochemical experiments with the π-conjugated bridge, namely 1,4-diphenylbutadiyne (**Figure 2d**), and the non-substituted •PTM (**Figure 2f**), were performed to elucidate the electronic structure of **2-R-Ox**. The UV-Vis spectrum of **2-R-Ox** (**Figure 2e**) resulted to be an almost perfect superposition of the spectra recorded for the two references in neutral state. Furthermore, none of the new features related to their respective oxidized species appear in the electronic spectrum of **2-R-Ox**. Consequently, the double bond of the stilbene unit turns out to be the only fragment in **2-R** where the removal of an electron during the first oxidation process could take place. In fact, the reactivity of stilbene derivatives has long been a popular topic in literature.[29] Different paths for the generation of their relative radical cations have been exploited, from one-electron oxidant[30,31] to anodic oxidation[32,33] or photochemical methods.[34] On the other hand, the formation of covalent radical cation dimers resulting from stilbene radical cations with their neutral analogues has also been proved.[34–37]

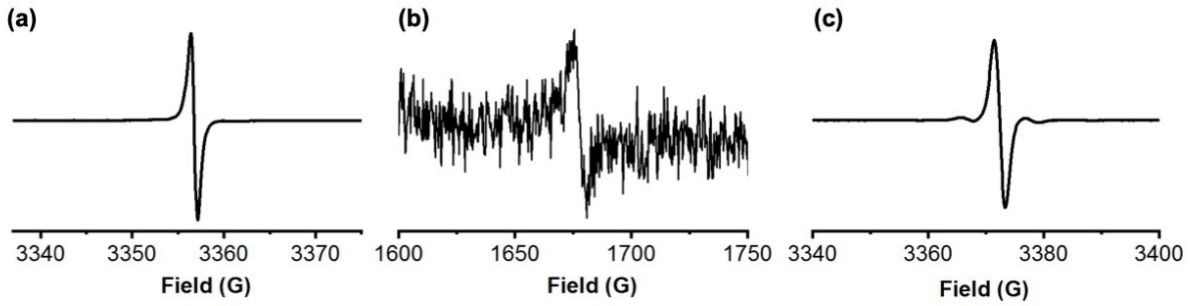

Figure 3. (a) ESR spectra of **2-R-Ox** in solution (9×10^{-4} M in DCM) at room temperature (b) ESR spectrum in frozen solution (130 K) showing the half-field signal centered at ~1678 G. (c) ESR spectra of **1-R-Ox** (9×10^{-4} M in DCM) at room temperature.

Chemical oxidations with $NOBF_4$ were performed for further characterization of the **2-R-Ox** species (Section 7, SI). Strikingly, the resulting ESR spectrum, a single narrow line was observed (**Figure 3**, ΔH_{pp}=1.0 G at g = 2.0031) in comparison with the three-line spectrum shown in **Figure 2a** for **2-R** (see a detailed analysis in **Figure S9**). As in the case of **1-R-Ox** (**Figure 3c**), these results clearly indicated a lack of coupling between the •PTM unpaired electron and its neighboring vinylene protons. Thus, the generation of a charge defect in **2-R-Ox**, as well as in **1-R-Ox**, mainly affecting their vinylene bridges was corroborated. Contrary to previous studies,[13] the formation of a closed-shell configuration due to the coupling between the unpaired electron of the •PTM radical

and the one generated in the bridge was discarded because the •PTM remains unaltered upon oxidation. It is known that radical cations from stilbene derivatives can be stabilized through dimer radical-cation structures formed with neutral molecules.[34,38] Further to this, the dimerization process is remarkably enhanced when a charge-spin separation takes place, through the contribution of a quinoid-type structure.[39] Taking all this into account, the formation of magnetically active dimers or larger oligomers upon oxidation of **1-R** and **2-R**, respectively, was proposed. Unfortunately, neither the isolation of the principal oxidized species nor the growing of appropriate monocrystals for X-ray diffraction could be attained despite the numerous attempts performed.

To assess the structure of the principal oxidized species, theoretical calculations were performed within the density functional theory (DFT) framework (Section 9, SI). The dimer formed by **1-R-Ox** and neutral **1-R** (*i.e.*, $[\mathbf{1\text{-}R}]_2^{\bullet+}$) was taken as a model case study, given the similarities revealed with **2-R-Ox**. DFT calculations at the M06-2X-D3/6-31G** level were first performed on a hypothetical structure **A** for $[\mathbf{1\text{-}R}]_2^{\bullet+}$, in which two molecules of **1-R** are bonded through two bridging ethylene carbon atoms to form a σ-type adduct (**Figure 4a**). Mulliken charge analysis, spin density, and bond distances demonstrate that structure **A** fits to a cationic dimer where one

•PTM unit adopts a closed-shell quinoid form, whereas the radical spreads all over the other monomer of the **[1-R]$_2^{\bullet+}$** adduct, with a particularly large contribution on the vinylene carbon (**Figures S10** and **S11**). This description contradicts the ESR experiments, which clearly indicate that the unpaired electron of the •PTM unit decouples from any vinylene proton. Structure **A** actually corresponds to a transition state with a small imaginary frequency (**Figure S12**), which leads to the formation of a cyclopropane ring in the so-called structure **B** (**Figure 4b**). Structure **B** is calculated 14.5 kcal mol^{-1} more stable than **A**, and is an absolute minimum in the potential energy surface. In structure **B**, the positive charge is mainly localized over one phenylacetylene moiety, as supported by bond distances (**Figure S13**) and Mulliken charge analysis (**Figure S14**), and the spin density is highly localized over one •PTM unit (**Figure 4c**). This suggests that the unpaired electron does not interact with the vinylene protons in the dimer, in good accord with the ESR data.

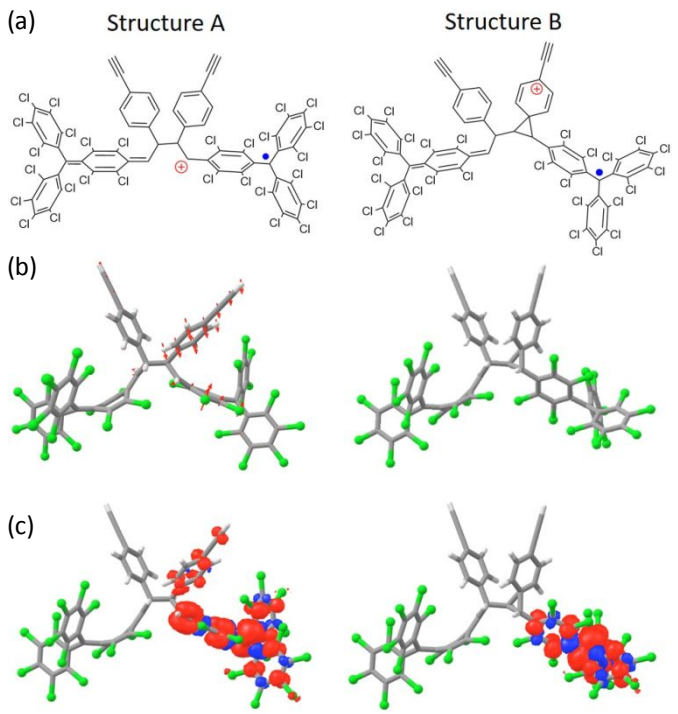

Figure 4. (a) Chemical structure, (b) minimum-energy optimized geometry and (c) Mulliken spin density calculated for structures **A** and **B** of dimer **[1-R]$_2^{\bullet+}$**. The vector displacements associated to the imaginary frequency of **A** leading to **B** are shown as red arrows in (b). Color coding: grey = C; green = Cl; white = H.

Hence, in line with previous studies,[13] the generation of **[1-R]$_2^{\bullet+}$** was necessarily mediated by the coupling between the unpaired electron of the •PTM and that generated on the vinylene spacer (**Scheme S4a**). Analogously, the same reactivity should be considered for **2-R-Ox**. However, since two stilbene units are present in **2-R**, a two-electron oxidation process might be foreseen, achieving a diradical tetrameric/oligomeric structure (**Scheme S4b**). Thus, once the intermolecular

interactions have been dismissed (**Figure S9**), the half-field signal recorded for **2-R-Ox** (**Figure 3b**) might come from the magnetically interacting diradical in which the triplet state is populated. Finally, the generation of larger structures hypothesized in **Scheme S4** was also experimentally supported by electrospray ionization (ESI) and matrix-assisted laser desorption ionization – time of flight (MALDI-ToF) measurements (Section 10, SI). For **1-R-Ox** and **2-R-Ox,** intense m/z peaks corresponding to heavier fragments than the neutral structures were observed.

In conclusion, a novel •PTM diradical derivative containing a 1,3-butadiyne bridge (**2-R**) was successfully synthesized. A detailed study on the positive and negative charged species of **2-R** was conducted, using both spectroscopic and electrochemical techniques, and compared to the monoradical **1-R** derivative. Upon reduction, a class-II anion-radical mixed-valence system has been generated successfully. Conversely, it has been demonstrated that, upon oxidation, neither the electron-rich bridge nor the •PTM radical moieties participate in the generation of the related radical cation (**2-R-Ox**). In fact, it has been proved that the oxidation process takes place in the vinylene linkers. Experimental and theoretical data support the mechanism here proposed: the resulting oxidized radical cation intermediates are stabilized by the •PTM units through quinoidal charged structures that further react with neutral diradicals to form big aggregates. This work

contributes to expanding the knowledge on the electrochemical reactivity of stilbene-based compounds and, in particular, the stabilizing role of neighboring persistent organic radicals.

ASSOCIATED CONTENT

Supporting Information. The Supporting Information is available free of charge. Synthetic procedures of all the compounds are detailed in the Supporting Information file, together with the most relevant ^{1}H-NMR, ^{13}C-NMR, FT-IR, ESR, and UV-Vis data. Considering the charged species here described, additional ESR and spectroelectrochemical data are also shown, as well as MALDI-ToF and ES+ ToF MS results and a description of the mixed-valence behavior. DFT calculations for **1-R-Ox** (geometry, charge, and spin analysis, and absorption spectra) are included (PDF).

AUTHOR INFORMATION

Notes

The authors declare no competing financial interests.

ACKNOWLEDGMENT

This work was supported by the MICINN of Spain (projects CTQ2016-80030-R, PGC2018-099568-B-I00 (EU Feder Funds), PID2019-111682RB-I00, Severo Ochoa FUNFUTURE CEX2019-000917-S, and María de Maeztu CEX2019-000919-M), the Generalitat de Catalunya (2017-SGR-918), the Generalitat Valenciana (PROMETEO/2020/077), and by the Networking Research Center on Bioengineering, Biomaterials and Nanomedicine (CIBER-BBN) Development Fund. P.M.B. gratefully thanks financial support from the Juan de la Cierva-Formación 2015 programme (FJCI-2015-23577) supported by MICINN. F.B. thanks the MECD for a predoctoral FPU fellowship. J.C. acknowledges the Generalitat Valenciana (APOSTD/2017/081). JAdS is enrolled in the Materials Science doctoral program of the UAB. JAdS thanks the MINECO for the FPI-SO fellowship. The authors acknowledge A. Bernabé from ICMAB for the MALDI-ToF measurements and Dr. Mireia Díaz and Dr. Marta Vilaseca, from the IRB Barcelona Mass Spectrometry and Proteomics Core Facility (unity member of ProteoRed, PRB3-ISCIII, supported by grant PRB3 (IPT17/0019-ISCIII-SGEFI / ERDF), for the ES+ ToF MS experiments. The work in Durham was supported by the EC FP7 ITN project MOLESCO (606728).

REFERENCES

(1) James, D. K.; Tour, J. M. Molecular Wires. In: Molecular Wires and Electronics. Topics in Current Chemistry, Vol. 257. Springer, Berlin, Heidelberg, 2005.

(2) Lathiotakis, N. N.; Theodorakopoulos, G.; Petsalakis, I. D. Electron Transfer through Organic Molecular Wires: A Theoretical Study. *Chem. Phys. Lett.* **2017**, *667*, 45–50.

(3) Sikes, H. D. Rapid Electron Tunneling Through Oligophenylenevinylene Bridges. *Science.* **2001**, *291* (5508), 1519–1523.

(4) Franco, C.; Burrezo, P. M.; Lloveras, V.; Caballero, R.; Alcón, I.; Bromley, S. T.; Mas-Torrent, M.; Langa, F.; López Navarrete, J. T.; Rovira, C.; *et al.* Operative Mechanism of Hole-Assisted Negative Charge Motion in Ground States of Radical-Anion Molecular Wires. *J. Am. Chem. Soc.* **2017**, *139* (2), 686–692.

(5) Tanaka, Y.; Kato, Y.; Tada, T.; Fujii, S.; Kiguchi, M.; Akita, M. "Doping" of Polyyne with an Organometallic Fragment Leads to Highly Conductive Metallapolyyne Molecular Wire. *J. Am. Chem. Soc.* **2018**, *140* (32), 10080–10084.

(6) Bryce, M. R. A Review of Functional Linear Carbon Chains (Oligoynes, Polyynes, Cumulenes) and Their Applications as Molecular Wires in Molecular Electronics and Optoelectronics. *J. Mater. Chem. C* **2021**. Advance Article.

(7) Wielopolski, M.; Santos, J.; Illescas, B. M.; Ortiz, A.; Insuasty, B.; Bauer, T.; Clark, T.; Guldi, D. M.; Martín, N. Vinyl Spacers—Tuning Electron Transfer through Fluorene-Based Molecular Wires. *Energy Environ. Sci.* **2011**, *4* (3), 765.

(8) Heckmann, A.; Lambert, C. Organic Mixed-Valence Compounds: A Playground for Electrons and Holes. *Angew. Chemie Int. Ed.* **2012**, *51* (2), 326–392.

(9) Souto, M.; Lloveras, V.; Vela, S.; Fumanal, M.; Ratera, I.; Veciana, J. Three Redox States of a Diradical Acceptor–Donor–Acceptor Triad: Gating the Magnetic Coupling and the Electron Delocalization. *J. Phys. Chem. Lett.* **2016**, *7* (12), 2234–2239.

(10) Veciana, J.; Riera, J.; Castañer, J.; Ferrer, N. Synthesis and Properties of the Complex of 1,4,7,10,13,16-Hexaoxacyclooctadecane with Potassium Perchlorotriphenylmethide. *J. Organomet. Chem.* **1985**, *297* (2), 131–141.

(11) Ballester, M.; Miravitlles, C.; Molins, E.; Carreras, C. Oxidation of the Perchlorotriphenylmethyl Radical to the Carbocation, and Its Unique Abrupt Reversion. *J. Org. Chem.* **2003**, *68* (7), 2748–2751.

(12) Souto, M.; Cui, H.; Peña-Álvarez, M.; Baonza, V. G.; Jeschke, H. O.; Tomic, M.; Valentí, R.; Blasi, D.; Ratera, I.; Rovira, C.; Veciana, J. Pressure-Induced Conductivity in a Neutral

Nonplanar Spin-Localized Radical. *J. Am. Chem. Soc.* **2016**, *138* (36), 11517–11525.

(13) Mayorga Burrezo, P.; Franco, C.; Caballero, R.; Mas-Torrent, M.; Langa, F.; López Navarrete, J. T.; Rovira, C.; Veciana, J.; Casado, J. Oligothienylenevinylene Polarons and Bipolarons Confined between Electron-Accepting Perchlorotriphenylmethyl Radicals. *Chem. Eur. J.* **2018**, *24* (15), 3776–3783.

(14) Shu, C.-H.; Liu, M.-X.; Zha, Z.-Q.; Pan, J.-L.; Zhang, S.-Z.; Xie, Y.-L.; Chen, J.-L.; Yuan, D.-W.; Qiu, X.-H.; *et al.* On-Surface Synthesis of Poly(p-Phenylene Ethynylene) Molecular Wires via in Situ Formation of Carbon-Carbon Triple Bond. *Nat. Commun.* **2018**, *9* (1), 2322.

(15) Biswas, M.; Nguyen, P.; Marder, T. B.; Khundkar, L. R. Unusual Size Dependence of Nonradiative Charge Recombination Rates in Acetylene-Bridged Compounds. *J. Phys. Chem. A* **1997**, *101* (9), 1689–1695.

(16) Sukegawa, J.; Schubert, C.; Zhu, X.; Tsuji, H.; Guldi, D. M.; Nakamura, E. Electron Transfer through Rigid Organic Molecular Wires Enhanced by Electronic and Electron–Vibration Coupling. *Nat. Chem.* **2014**, *6* (10), 899–905.

(17) Abe, M. Diradicals. *Chem. Rev.* **2013**, *113* (9), 7011–7088.

(18) Hu, X.; Wang, W.; Wang, D.; Zheng, Y. The Electronic Applications of Stable Diradicaloids: Present and Future. *J. Mater. Chem. C* **2018**, *6* (42), 11232–11242.

(19) Bejarano, F.; Olavarria-Contreras, I. J.; Droghetti, A.; Rungger, I.; Rudnev, A.; Gutiérrez, D.; Mas-Torrent, M.; Veciana, J.; van der Zant, H. S. J.; Rovira, C.; *et al.* Robust Organic Radical Molecular Junctions Using Acetylene Terminated Groups for C–Au Bond Formation. *J. Am. Chem. Soc.* **2018**, *140* (5), 1691–1696.

(20) Bettanin, L.; Botteselle, G. V.; Godoi, M.; Braga, A. L. Green Synthesis of 1,3-Diynes from Terminal Acetylenes under Solvent-Free Conditions. *Green Chem. Lett. Rev.* **2014**, *7* (2), 105–112.

(21) Lloveras, V.; Vidal-Gancedo, J.; Figueira-Duarte, T. M.; Nierengarten, J.-F.; Novoa, J. J.; Mota, F.; Ventosa, N.; Rovira, C.; Veciana, J. Tunneling versus Hopping in Mixed-Valence Oligo- p -Phenylenevinylene Polychlorinated Bis(Triphenylmethyl) Radical Anions. *J. Am. Chem. Soc.* **2011**, *133* (15), 5818–5833.

(22) Sporer, C.; Ratera, I.; Ruiz-Molina, D.; Zhao, Y.; Vidal-Gancedo, J.; Wurst, K.; Jaitner, P.; Clays, K.; Persoons, A.; Rovira, C.; Veciana, J. A Molecular Multiproperty Switching Array Based on the Redox Behavior of a Ferrocenyl Polychlorotriphenylmethyl Radical. *Angew.*

Chemie Int. Ed. **2004**, *43* (39), 5266–5268.

(23) Simão, C.; Mas-Torrent, M.; Crivillers, N.; Lloveras, V.; Artés, J. M.; Gorostiza, P.; Veciana, J.; Rovira, C. A Robust Molecular Platform for Non-Volatile Memory Devices with Optical and Magnetic Responses. *Nat. Chem.* **2011**, *3* (5), 359–364.

(24) Crivillers, N.; Mas-Torrent, M.; Vidal-Gancedo, J.; Veciana, J.; Rovira, C. Self-Assembled Monolayers of Electroactive Polychlorotriphenylmethyl Radicals on Au(111). *J. Am. Chem. Soc.* **2008**, *130* (16), 5499–5506.

(25) Ratera, I.; Veciana, J. Playing with Organic Radicals as Building Blocks for Functional Molecular Materials. *Chem. Soc. Rev.* **2012**, *41* (1), 303–349.

(26) Rovira, C.; Ruiz-Molina, D.; Elsner, O.; Vidal-Gancedo, J.; Bonvoisin, J.; Launay, J.-P.; Veciana, J. Influence of Topology on the Long-Range Electron-Transfer Phenomenon. *Chem. Eur. J.* **2001**, *7* (1), 240–250.

(27) Bonvoisin, J.; Launay, J.-P.; Rovira, C.; Veciana, J. Purely Organic Mixed-Valence Molecules with Nanometric Dimensions Showing Long-Range Electron Transfer. Synthesis, and Optical and EPR Studies of a Radical Anion Derived from a Bis(Triarylmethyl)Diradical. *Angew. Chemie Int. Ed. English* **1994**, *33* (20), 2106–2109.

(28) Sedó, J.; Ruiz, D.; Vidal-Gancedo, J.; Rovira, C.; Bonvoisin, J.; Launay, J.-P.; Veciana, J. Intramolecular Electron Transfer Phenomena in Purely Organic Mixed-Valence High-Spin Ions: A Triplet Anion Case. *Adv. Mater.* **1996**, *8* (9), 748–752.

(29) Likhtenshtein, G. *Stilbenes*; Wiley-VCH Verlag GmbH & Co. KGaA: Weinheim, Germany, 2009.

(30) Li, W.; Chen, P.; Yang, Y.; Liu, X.; Dong, T. Synthesis of Diverse Oligostilbenes from FeCl 3 -Mediated Oxidation of Protected Resveratrol. *Tetrahedron* **2016**, *72* (1), 210–215.

(31) Velu, S. S.; Buniyamin, I.; Ching, L. K.; Feroz, F.; Noorbatcha, I.; Gee, L. C.; Awang, K.; Wahab, I. A.; Weber, J. F. F. Regio- and Stereoselective Biomimetic Synthesis of Oligostilbenoid Dimers from Resveratrol Analogues: Influence of the Solvent, Oxidant, and Substitution. *Chem. Eur. J.* **2008**, *14* (36), 11376–11384.

(32) Hong, F. J.; Low, Y. Y.; Chong, K. W.; Thomas, N. F.; Kam, T. S. Biomimetic Oxidative Dimerization of Anodically Generated Stilbene Radical Cations: Effect of Aromatic Substitution on Product Distribution and Reaction Pathways. *J. Org. Chem.* **2014**, *79* (10), 4528–4543.

(33) Yan, M.; Kawamata, Y.; Baran, P. S. Synthetic Organic Electrochemical Methods Since

2000: On the Verge of a Renaissance. *Chem. Rev.* **2017**, *117* (21), 13230–13319.

(34) Lewis, F. D.; Bedell, A. M.; Dykstra, R. E.; Elbert, J. E.; Gould, I. R.; Farid, S. Photochemical Generation, Isomerization, and Oxygenation of Stilbene Cation Radicals. *J. Am. Chem. Soc.* **1990**, *112* (22), 8055–8064.

(35) Akaba, R.; Sakuragi, H.; Tokumaru, K. Detection of Dimeric Radical Cations of Trans-Stilbene in 2,4,6-Triphenylpyrylium Tetrafluoroborate-Sensitized Electron Transfer Reactions in Dichloromethane. *Chem. Phys. Lett.* **1990**. *174* (1), 80-84.

(36) Majima, T.; Tojo, S.; Ishida, A.; Takamuku, S. Reactivities of Isomerization, Oxidation, and Dimerization of Radical Cations of Stilbene Derivatives. *J. Phys. Chem.* **1996**, *100* (32), 13615–13623.

(37) Majima, T.; Tojo, S.; Ishida, A.; Takamuku, S. Cis − Trans Isomerization and Oxidation of Radical Cations of Stilbene Derivatives. *J. Org. Chem.* **2002**, *61* (22), 7793–7800.

(38) Steckhan, E. Spectroelectrochemical Studies of Olefins. 3. The Dimerization Mechanism of the 4,4'-Dimethoxystilbene Cation Radical in the Absence and Presence of Methanol. *J. Am. Chem. Soc.* **1978**, *100* (11), 3526–3533.

(39) Majima, T.; Tojo, S.; Ishida, A.; Takamuku, S. Reactivities of Isomerization, Oxidation,

and Dimerization of Radical Cations of Stilbene Derivatives. *J. Phys. Chem.* **1996**, *100* (32), 13615–13623.

Supporting information for

Allocation of Ambipolar Charges on an Organic Diradical with a Vinylene-Phenylenediyne Bridge

Paula Mayorga-Burrezo,[†] *Francesc Bejarano,*[†] *Joaquín Calbo,*[§] *Xiaotao Zhao,*[¶] *J. Alejandro de Sousa,*[†+] *Vega Lloveras,*[†] *Martin R. Bryce,*[¶] *Enrique Ortí,**[§]*Jaume Veciana,**[†] *Concepció Rovira,**[†] *Núria Crivillers**[†]

[†]Institut de Ciència de Materials de Barcelona, ICMAB-CSIC, Campus UAB, 08193 Bellaterra, Spain

[§]Instituto de Ciencia Molecular, Universidad de Valencia, Catedrático José Beltrán, 2, 46980 Paterna, Spain

[¶]Chemistry Department, Durham University, Durham DH1 3LE, U.K.

[+]Laboratorio de Electroquímica, Departamento de Química, Facultad de Ciencias, Universidad de los Andes, 5101 Mérida, Venezuela.

Content

1. Materials & Apparatus

All the commercial reagents and electrolytic salts were purchased from Sigma-Aldrich and utilized without any further purification. HPLC grade solvents were exclusively used. Anhydrous THF and toluene were distilled over Na/benzophenone prior to their use, and anhydrous dichloromethane was obtained from its distillation with CaH_2.

Cyclic voltammetry (CV) and dynamic pulse voltammetry (DPV) characterization was performed with an AUTOLAB 204 with NOVA 1.9 software, by means of a custom built electrochemical cell. Pt wires were used as working and counter electrodes, whereas an Ag wire was chosen as pseudo-reference electrode. An electrolyte solution of 0.2 M tetrabutylammonium hexafluorophosphate ($TBAPF_6$) in dry CH_2Cl_2 under argon atmosphere was used in both measurements. Ferrocene was employed as internal reference. In-situ UV-Vis-NIR spectroelectrochemical studies were conducted on a Varian Cary 5000 UV-Vis-NIR spectrometer with a thin-layer cell from a demountable omni cell from Specac. The spectra were collected at constant potential electrolysis. On the other hand, Quartz cuvettes with an optical path of 1 cm were used for UV-Vis absorption spectroscopy measurements.

Electron spin resonance (ESR) spectra were registered on a Bruker ESP 300 E spectrometer provided with a rectangular cavity T102 working with a X band (9.5 GHz). Precaution to avoid undesirable spectra distortion and line broadening, such as those arising from microwave power saturation and magnetic field over modulation, were also taken into account. To avoid dipolar line broadening from dissolved oxygen, solutions were always carefully degassed with Argon.

High-performance liquid chromatography (HPLC) analyses were carried out in reversed-phase mode using an Agilent 1260 Infinity II chromatograph provided with a diode array detector WR and a quaternary pump VL. The column used was TRACER EXCEL 120 ODSA 5 µm 25x0.46 from Teknokroma. The same non-isocratic method was used for all compounds with an acetonitrile/chloroform mixture (total time = 15 min; t = 0 min 90:10, t = 7 min 60:40, t = 13 min 60:40, t = 14 min 90:10).

Nuclear magnetic resonance spectroscopy (NMR), particularly ^{1}H-NMR and ^{13}C-NMR spectra, were registered on a Bruker Avance III 400SB spectrometer and calibrated using residual undeuterated dichloromethane ($\delta(^1H)$ = 5.32 ppm; $\delta(^{13}C)$ = 53.84 ppm) and residual undeuterated chloroform ($\delta(^1H)$ = 7.26 ppm; $\delta(^{13}C)$ = 77.00 ppm) as internal references. The data analysis was carried out with MestReNova software (MestReLab Research S. L.). The following abbreviations were used to designate multiplicities: br = broad signal, s = singlet, d = doublet, m = multiple. Finally, infrared spectroscopy (IR) spectra were registered with a FT-IR PerkinElmer spectrometer with a diamond ATR accessory.

The matrix-assisted laser desorption ionization – time-of-flight (MALDI/ToF) mass spectrometry (MS) spectrum of **2-R-Ox** was recorded in a Bruker Ultraflex LDI-TOF spectrometer from a DCM solution.

Positive electrospray ionization time-of-flight mass spectrometry (ES+ ToF MS) experiments were performed on a Synapt G1 HDMS mass spectrometer (Waters, Manchester, UK). The sample was placed on a 384-well plate refrigerated at 15 ºC and introduced by automated chip-base nanoelectrospray using a Triversa NanoMate (Advion BioSciences) in positive ion mode Sampling cone 60V backing 2.26e0. The instrument was calibrated over the m/z range 400–8000, using a solution of cesium iodide. MassLynx *vs.* 4.1 SCN 704 and Driftscope *vs.* 2.1 softwares were used for mass spectrometry data processing. **2-R-Ox** was dissolved in a pure DCM in order to preserve the stability of the charged species.

2. General procedures

Reactions to synthesize the different compounds were monitored by thin-layer chromatography (TLC) carried out on 250 µm Sigma-Aldrich silica gel plates (60F-254) using UV light as visualizing agent and a basic solution and heat as developing agents. Reactions to obtain radical compounds were monitored by UV-Vis spectroscopy. Purification of all compounds was carried out by flash column chromatography using Carlo Erba silica gel (60, particle size 35–70 µm).

(*E*)-6,6'-((2,3,5,6-tetrachloro-4-(4-ethynylstyryl)phenyl)methylene)*bis*(1,2,3,4,5-pentachloro-benzene) was synthesized following the reported procedures.[1]

3. Synthesis details and characterization of the PTM derivatives

Scheme S1. *Synthesis of* ***2-R****.*

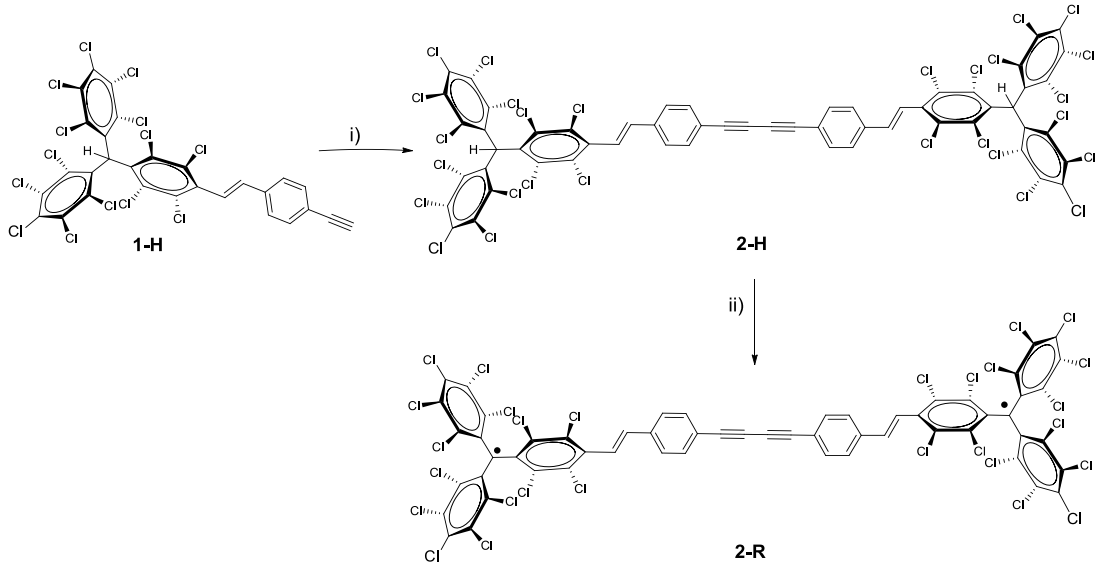

[a]Reagents and conditions: (i) CuCl, TMEDA / DMF(100 ºC, 100 W), (ii) Bu_4NOH/THF then *p*-chloranil (rt)

(a) Compound 2-H

The synthesis and purification of compound 1,4-bis(4-((E)-4-(bis(perchlorophenyl)methyl)-2,3,5,6-tetrachlorostyryl)phenyl)-buta-1,3-diyne (**2-H** in **Scheme S1)** was carried out under red light to avoid trans-cis isomerization. Two different synthetic routes were followed:

Route A: Compound **1-H** (99 mg, 0.116 mmol), CuCl (3.6 mg, 0.036 mmol), tetramethylethylenediamine (TMEDA, 40 µL, 0.267 mmol) and anhydrous DMF (1 mL) were placed in a vessel. The resulting dark green suspension was stirred in a microwave oven for 30 minutes, keeping temperature at 100 °C, applying a maximum power of 100 watts and under atmospheric pressure. Then, the reaction was quenched upon addition of aqueous 0.4 M HCl drops until a brown suspension was obtained. The product was extracted with DCM (3 x 5 mL) and the combined organic layers were washed with brine until complete removal of DMF. Afterwards, the organic phase was dried over anhydrous magnesium sulfate, filtered and evaporated under vacuum. The resulting crude product was purified by column chromatography (SiO_2, hexanes/DCM 9:1) giving rise to the pure compound **2-H** as a yellow powder (74 mg, 74% yield).

Route B:

First, in a round-bottom flask equipped with a reflux condenser and a $CaCl_2$ tube on top, a solution of $Cu(OAc)_2$ (968.0 mg 5.33 mmol) and K_2CO_3 (827.7 mg, 5.99 mmol) in an anhydrous mixture of MeOH/pyridine 1:1 (40 mL) was heated at 60 ºC **(Solution 1).**

Then, in another flask, compound **1-H** (150.4 mg, 0.18 mmol) and CuCl (18.5, 0.19 mmol) were dissolved in anhydrous pyridine (10 mL) and then MeOH (10 mL) was added. The resulting solution was added dropwise to the **solution 1**, and the reaction mixture was stirred at 60 ºC overnight. Afterwards, aqueous 2 M HCl (200 mL) and CH_2Cl_2 (100 mL) were added. After the phases separation, the aqueous phase was extracted with additional CH_2Cl_2 (100 mL). The combined organic phases were washed with aqueous 2 M HCl (2 x 100 mL), dried over anhydrous magnesium sulfate, filtered and evaporated under vacuum. The obtained crude product was purified by column chromatography (SiO_2, hexane/DCM 90:10) to give the desired product as a yellow powder (138.1 mg, 92% yield).

Compound **2-H** was also isolated as side-product from the synthesis of compounds **3** and **5** (**Scheme S2**) in a 37% and 30% yield respectively.

^{1}H-NMR (400 MHz, CD_2Cl_2): δ = 7.59 (d, 4H, ArC-H, ^3J = 8.8 Hz), 7.56 (d, 4H, ArC-H, ^3J = 8.8 Hz), 7.14 (d, 2H , ^3J = 16.6 Hz, H−C=CH), 7.08 (d, 2H, ^3J = 16.6 Hz, H−C=C−H), 7.04 (s, 2H, α-H) ppm; **^{13}C-NMR** (101 MHz, CD_2Cl_2): δ = 137.80, 137.59, 137.42, 137.02, 136.70, 135.54, 135.47, 135.28, 134.46, 134.39, 133.98, 133.94, 133.91, 133.86, 133.35, 132.89, 132.74, 127.39, 125.04, 122.24, 82.50 (C≡C, 75.38 (C≡C), 57.09 (α-C) ppm; **ATR-IR**: (cm^{-1}) = 3037 (w) (ArCH), 1635 (w) (C=C), 1600 (w), 1534 (w) (ArC−ArC), 1517 (w)

(ArC−ArC), 1503 (w) (ArC−ArC), 1362 (m) (Cl−ArC−ArC−Cl), 1339 (m) (Cl−ArC−ArC−Cl), 1295 (m) (Cl−ArC−ArC−Cl), 1239 (w), 1208 (w), 1192 (w), 1139 (w), 1120 (w), 1016 (w), 967 (w), 947 (w), 872 (w), 857 (w), 808 (s) (C−Cl), 715 (w), 699 (w), 689 (w), 671 (m), 649 (m), 614 (w), 607 (w), 578 (w), 559 (w), 537 (w), 529 (w); **MS (ESI)**: *m/z* 1702.3 [M – H]-; **UV-Vis** (THF): λ (nm) (ξ, M^{-1} cm^{-1}) 238 (115887), 326 (50380), 357 (83566).

(b) Compound 2-R

The synthesis of compound 1,4-bis(4-((E)-4-(bis(perchlorophenyl)methyl)-2,3,5,6-tetrachlorostyryl)phenyl)-buta-1,3-diyne diradical (**2-R** in **Scheme S1**) was carried out under red light. Compound **2-H** (106 mg, 0.062 mmol) was dissolved in a mixture of toluene (3.5 mL) and THF (8.5 mL) previously filtered through neutral Al_2O_3. 54–56 % aqueous TBAOH (100 µL, 0.21 mmol) was added and the solution was stirred. The formation of the perchlorotriphenylmethide dianion was monitored by UV-Vis absorption spectroscopy. When the deprotonation was complete (about 20 minutes), *p*-chloranil was added (56 mg, 0.23 mmol), and the oxidation from the triphenylmethide dianion to the dirradical was followed by UV-Vis absorption spectroscopy. When the oxidation was complete (about 4 hours), the mixture was evaporated under vacuum, and the crude product was purified by column chromatography (SiO_2, hexanes/DCM 100:0 → 80:20) to afford the pure diradical **2-R** as a dark green powder (96 mg, 91% yield). **ATR-IR**: (cm^{-1}) 3033 (w) (ArC−H), 1627 (w) (C=C), 1598 (w), 1505 (w) (ArC−ArC), 1465 (w) (ArC−ArC), 1410 (w), 1335 (s) (Cl−ArC−ArC−Cl), 1321 (s) (Cl−ArC−ArC−Cl), 1292 (m) (Cl−ArC−ArC−Cl), 1259 (m) (Cl−ArC−ArC−Cl), 1224 (w), 1157 (w), 1120 (w), 1082 (w), 1047 (w), 1015 (w), 968 (w), 945 (w), 907 (w), 874 (w), 856 (w), 815 (s) (C−Cl), 776 (w), 736 (m), 708 (m), 653 (s), 621 (w), 605 (w), 593 (w), 537 (w); **EM (ESI)**: *m/z* 1701.4 [M]-; **UV-Vis** (THF): λ (nm) (ξ, M^{-1} cm^{-1}) 267 (35521), 348 (57529), 368 (66774), 386 (80785), 459 (27558), 565 (3610), 619 (3099); **CV** (0.2 M TBAPF6 in DCM, *vs* Fc/Fc+): $E^{1/2}$ = –0.52 V, $E^{1/2}$ = 1.05 V, $E^{1/2}$ = 1.29 V; **ESR**: g = 2.0030, a(^{1}HPTM−C=CH) = 0.9 G, a(^{1}HPTM−CH=CH) = 0.2 G, ΔHpp = 0.7 G, a(α-^{13}C) = 14.8 G, a(Ar^{13}C) = 5.3 G; **SQUID**: C = 0.74 $cm^3 \cdot K \cdot mol^{-1}$, g = 1.968.

(c) Longer polyalkyne-bridged PTM derivatives

Caution: Care should be taken when handling longer oligo/polyynes and their intermediates in bulk quantities due to their potential explosive instability. The longer members of the polyalkyne-bridged PTM derivatives were synthesized by direct dimerization of trimethylsilyl (TMS)-protected alkyne monomers, as depicted in **Scheme S2**.

Scheme S2. *Synthesis of* ***4-H*** *and* ***6-H***

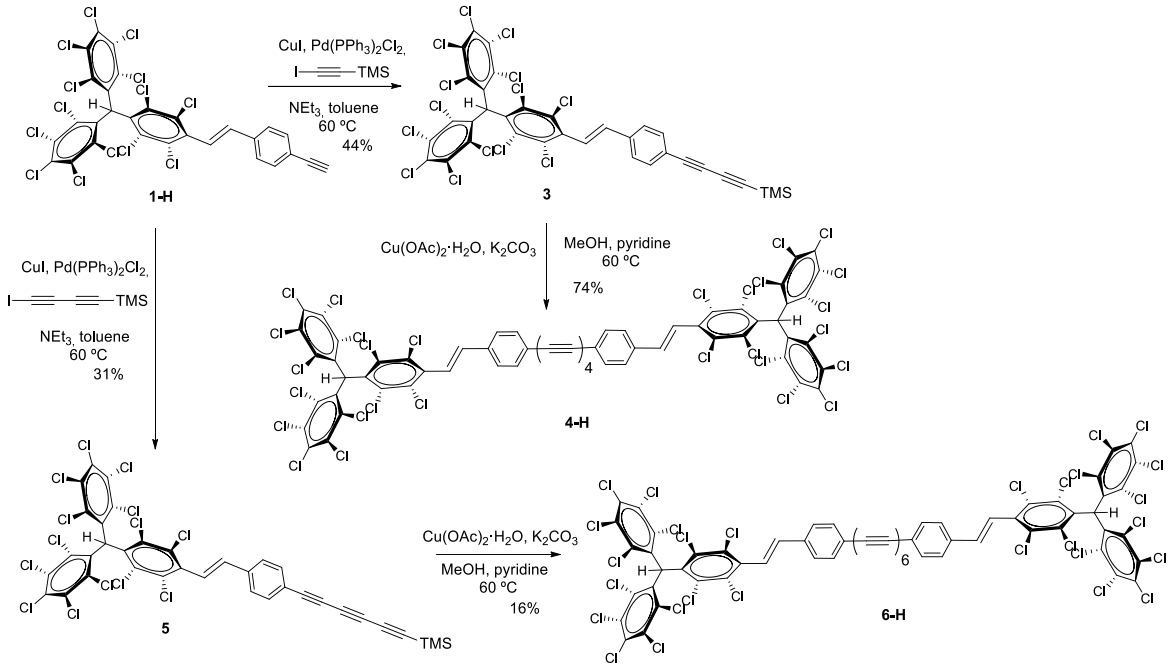

(c.1) Compound 3

The synthesis and purification of this compound ((*E*)-((4-(4-(bis(perchlorophenyl)methyl)-2,3,5,6-tetrachlorostyryl)phenyl)buta-1,3-diyn-1-yl)trimethylsilane (**3** in **Scheme S2**)) was carried out under red light. Compound **1-H** (680 mg, 0.80 mmol), CuI (35 mg, 0.18 mmol) and $Pd(PPh_3)_2Cl_2$ (56 mg, 0.08 mmol) were suspended in dry THF (1.5 mL) under N_2 atmosphere in a Schlenk flask which was placed at 60 ºC. 1-iodo-2-(trimethylsilyl)acetylene (250 µL, 1.63 mmol) and anhydrous NEt_3 (12 mL, 84 mmol) were subsequently added in this order and the reaction was stirred at 60 ºC overnight. Then, the crude product was evaporated under vacuum, dissolved again in DCM, and filtered. The filtrate was evaporated again. The obtained crude product was purified by column chromatography (SiO_2, hexanes/DCM 100:0 → 95:5) affording the pure product **3** as a yellowish powder (331 mg, 44% yield) and compound **1-H** (250 mg). **^{1}H-NMR** (400 MHz, CD_2Cl_2): δ = 7.53 (m, 4H, ArC−H), 7.12 (d, 1H , 3*J* = 16.5 Hz, H−C=C−H), 7.06 (d, 1H, 3*J* = 16.5 Hz, H−C=C−H), 7.03 (s, 1H, *α*-H), 0.23 (s, 9H, CH_3) ppm; **^{13}C-NMR** (101 MHz, CD_2Cl_2): δ = 137.77, 137.57, 137.43, 137.02, 137.01, 136.69, 135.54, 135.46, 135.27, 134.45, 134.38, 133.99, 133.97, 133.93, 133.90, 133.84, 133.51, 132.88, 132.88, 132.73, 127.33, 125.05, 124.96, 123.94, 121.91, 92.12 (CΞC), 87.88 (CΞC), 76.76 (CΞC), 75.69 (CΞC), 57.07 (*α*-C), -0.35 (-CH_3) ppm; **ATR-IR**: (cm^{-1}) = 3082 (w) (ArC−H), 3065 (w) (ArC−H), 3044 (w) (ArC−H), 2200 (w) (CΞC), 2101 (w) (CΞC), 1632 (w) (C=C), 1602 (w), 1533 (w) (ArC−ArC), 1508 (w) (ArC−ArC), 1412 (w), 1363 (m) (Cl−ArC−ArC−Cl), 1339 (m) (Cl−ArCArC−Cl), 1296 (m) (Cl−ArC−ArC−Cl), 1249 (m) (Cl−ArC−ArC−Cl), 1207 (w), 1190 (w), 1139 (w), 1119 (w), 1030 (w), 1011 (w), 967 (w), 947 (w), 841 (s), 808 (s) (C-Cl), 758 (m), 711 (w), 686 (m), 670 (m), 649 (m), 632 (w), 623 (w), 610 (w), 577 (w), 537 (w), 524 (w), 510 (m); **LDI-ToF** (negative mode): *m/z* 947.3 $[M – H]^–$, 877.4 $[M – 2 Cl – H]^–$; **UV-Vis** (THF): λ (nm) (ξ, M^{-1} cm^{-1}) 227 (92451), 238 (65596), 254 (29590), 310 (32780), 331 (49483).

(c.2) Compound 4-H

The synthesis and purification of 1,8-bis(4-((*E*)-4-(bis(perchlorophenyl)methyl)-2,3,5,6-tetrachlorostyryl)phenyl)-octa-1,3,5,7-tetrayne (**4-H** in **Scheme S2**) was carried out under red light. In a round-bottom flask equipped with a reflux condenser, $Cu(OAc)_2·H_2O$ (867 mg, 4.38 mmol) and K_2CO_3 (471 mg, 3.41 mmol) were dissolved in an anhydrous mixture of MeOH/pyridine 1:1 (20 mL) and the mixture was heated at 60 ºC with a $CaCl_2$ tube on top to close the system. In another flask, compound **3** (103 mg, 0.108 mmol) was dissolved in anhydrous pyridine (10 mL) and MeOH (10 mL) was added. The resulting solution was added dropwise to the $Cu(OAc)_2·H_2O$ and K_2CO_3 solution, and the reaction mixture was stirred at 60 ºC overnight. Afterwards, aqueous 0.4 M HCl (40 mL) and $CHCl_3$ (40 mL) were added. The phases were separated and the aqueous layer was extracted with additional $CHCl_3$ (40 mL). The combined organic layers

were washed with aqueous 0.4 M HCl (2 x 50 mL), dried over anhydrous magnesium sulfate, filtered, and evaporated under vacuum. The obtained crude product was purified by column chromatography (SiO_2, hexanes/ $CHCl_3$ 85:15 → 20:80) to give the desired product as a yellow-brown powder (74 mg, 74% yield). **^{1}H-NMR** (CD_2Cl_2, 400 MHz): *δ* = 7.57 (d, 4H, 3*J* = 8.5 Hz ArC−H), 7.51 (d, 4H, 3*J* = 8.5 Hz, ArC−H), 7.11 (d, 2H, 3*J* = 16.6 Hz, H−C=C−H), 7.05 (d, 2H, 3*J* = 16.6 Hz, H−C=C−H), 7.02 ppm (s, 2H, *α*-H); **^{13}C-NMR** (CD_2Cl_2, 101 MHz): *δ* = 138.17, 137.62, 137.45, 136.98, 136.77, 135.51, 135.45, 135.27, 134.43, 134.38, 134.10, 133.98, 133.96, 133.91, 133.89, 133.83, 132.87, 132.71, 131.30, 130.30, 129.47, 129.12, 128.58, 127.45, 125.53, 120.81, 78.30 (CΞC), 75.71 (CΞC), 67.97 (CΞC), 64.24 (CΞC), 57.00 (*α*-C); **ATR-IR**: (cm^{-1}) = 3030 (w) (ArC-H), 2332 (w), 2201 (w) (CΞC), 2190 (w) (CΞC), 1726 (w), 1632 (w) (C=C), 1598 (w), 1535 (w) (ArC−ArC), 1520 (w) (ArC−ArC), 1504 (w) (ArC−ArC), 1412 (w), 1361 (m) (Cl−ArC−ArC−Cl), 1340 (m) (Cl−ArC−ArC−Cl), 1331 (sh), 1299 (m) (Cl−ArC−ArC−Cl), 1289 (sh), 1262 (w), 1240 (w), 1210 (w), 1190 (w), 1139 (w), 1118 (w), 1108 (sh), 1016 (w), 969 (w), 948 (w), 937 (sh), 872 (w), 859 (w), 847 (sh), 818 (m), 807 (s) (C-Cl), 758 (w), 749 (w), 734 (w), 718 (w), 690 (m), 681 (m), 670 (m), 649 (m), 607 (w), 607 (w), 574 (w), 556 (w), 537 (w), 529 (w); **UV-Vis** (DCM): *λ* (nm) (*ξ*,M^{-1} cm^{-1}) 306 (57514), 322 (85289), 341 (117503), 362 (120622), 389 (125545), 423 (50154).

(c.3) Compound 5

The synthesis and purification of (*E*)-((4-(4-(bis(perchlorophenyl)methyl)-2,3,5,6-tetrachlorostyryl)pheyl)hexa-1,3,5-triyn-1-yl)trimethylsilane (**5** in **Scheme S2**) was carried out under red light. Compound **1-H** (570 mg, 0.67 mmol), CuI (37 mg, 0.19 mmol), and $Pd(PPh_3)_2Cl_2$ (44 mg, 0.08 mmol) were suspended in dry THF (1.5 mL) under N_2 atmosphere in a Schlenk flask which was placed at 60 ºC. (Iodobuta-1,3-diyn-1-yl)trimethylsilane (421 mg, 1.63 mmol) and anhydrous NEt_3 (11 mL, 77 mmol) were subsequently added and the reaction was stirred at 60 ºC overnight. Then, the solution was evaporated under vacuum, dissolved again in DCM, and filtered, and the filtrate was evaporated again. The obtained crude was purified by column chromatography (SiO_2, hexanes/DCM 100:0 → 95:5) affording the pure product **5** as a yellow-brown powder (203 mg, 31% yield) and compound **1-H** as biproduct (202 mg). **^{1}H-NMR** (400 MHz, CD_2Cl_2): *δ* = 7.57 (d, 2H, ArC−H, 3*J* = 8.4 Hz), 7.53 (d, 2H, ArC−H, 3*J* = 8.4 Hz), 7.13 (d, 1H , 3*J* = 16.7 Hz, H−C=C−H), 7.07 (d, 1H, 3*J* = 16.7 Hz, H−C=C−H), 7.04 (s, 1H, *α*-H), 0.23 (s, 9H, CH3) ppm; **^{13}C-NMR** (101 MHz, $CDCl_3$): *δ* = 137.90, 137.70, 137.50, 137.01, 137.00, 136.76, 135.55, 135.48, 135.31, 134.46, 134.41, 134.30, 134.02, 134.00, 133.94, 133.86, 132.90, 132.75, 127.42, 125.36, 121.21, 90.32 (CΞC), 87.98 (CΞC), 77.09 (CΞC), 75.70 (CΞC), 67.80 (CΞC), 61.56 (CΞC), 57.09 (*α*-C), -0.45 (CH_3) ppm; **ATR-IR**: (cm^{-1}) = 3033 (w) (C=CH), 2187 (w), 2176 (w), 2170 (w), 2163 (w), 2072 (w) (CΞC), 2047 (w), 1637 (w) (C=C), 1599 (w) , 1535 (w) (ArC−ArC), 1507 (w) (ArC−ArC), 1466 (w), 1455 (w), 1413 (w) (Cl−ArC−ArC−Cl), 1359 (w) (Cl−ArC−ArC−Cl), 1338 (m) (Cl−ArC−ArC−Cl), 1326 (m), 1297 (m), 1249 (m), 1206 (w), 1188 (w), 1138 (w), 1119 (w), 1016 (w), 970 (w), 948 (w), 864 (sh, m), 843 (s), 818 (s), 807 (s) (ArC−Cl), 760 (m), 745 (w), 723 (w), 721 (w), 704 (m), 691 (m), 682 (m), 671 (m), 648 (s), 615 (w), 607 (w), 563 (w), 539 (w), 530 (w), 519 (w), 506 (w), 502 (w); **LDI-ToF** (negative mode): *m/z* 972.4 $[M – H]^–$, 900.5 $[M – 2 Cl – H]^–$; **UV-Vis** (THF): *λ* (nm) (*ξ*, M^{-1} cm^{-1}) 261 (36027), 296 (32669), 314 (35509), 337 (52122), 360 (49763).

(c.4) Compound 6-H

The synthesis of 1,12-bis(4-((E)-4-(bis(perchlorophenyl)methyl)-2,3,5,6-tetrachlorostyryl)phenyl)-dodeca-1,3,5,7,9,11-hexayne (compound **6-H** in **Scheme S2**) was carried out under red light. In a round-bottom flask equipped with a reflux condenser, $Cu(OAc)_2·H_2O$ (850 mg, 4.27 mmol) and K_2CO_3 (450 mg, 3.26 mmol) were dissolved in an anhydrous mixture of MeOH/pyridine 1:1 (18 mL) and the mixture was heated at 60 ºC with a $CaCl_2$ tube on top to close the system. In another flask, compound **5** (85 mg, 0.087 mmol) was dissolved in anhydrous pyridine (9 mL) and MeOH (9 mL) was added. The resulting solution was dropwise added to the $Cu(OAc)_2·H_2O$ and K_2CO_3 solution, and the reaction mixture was stirred at 60 ºC for 6 hours. Afterwards, aqueous 0.4 M HCl (50 mL) and $CHCl_3$ (50 mL) were added, phases were separated, and the aqueous layer was extracted with additional $CHCl_3$ (40 mL). The combined organic layers were washed with aqueous 0.4 M HCl (2 x 50 mL), dried over anhydrous magnesium sulfate, filtered, and evaporated under vacuum. The obtained crude product was purified by column chromatography (SiO_2, hexanes/$CHCl_3$ 95:5 → 60:40) to give the product as an orange powder (24 mg, 16% yield). **^{1}H-NMR** ($CDCl_3$, 400 MHz): *δ* = 7.57 (d, 4H, 3*J* = 8.5 Hz, ArC−H), 7.50 (d, 4H, 3*J* = 8.5 Hz, ArC−H), 7.10 (d, 2H, 3*J* = 16.6 Hz, H−C=C−H), 7.04 (d, 2H, 3*J* = 16.6 Hz, H−C=C−H), 7.01 (s, 2H, *α*-H) ppm; **^{13}C-NMR** ($CDCl_3$, 101 MHz): *δ* = 137.85, 137.29,

136.89, 136.48, 136.06, 135.08, 135.04, 134.95, 134.00, 133.97, 133.95, 133.94, 133.70, 133.68, 133.55, 133.40, 132.51, 132.27, 130.96, 128.84, 127.43, 127.07, 125.13, 120.28, 77.26 (CΞC), 75.74 (CΞC), 68.07 (CΞC), 65.03 (CΞC), 63.81 (CΞC), 62.59 (CΞC), 56.64 (*α*-C); **ATR-IR**: (cm^{-1}) = 2112 (w) (CΞC), 2050 (w) (CΞC), 2039 (w) (CΞC), 1637 (w) (C=C), 1542 (w) (ArC−ArC), 1508 (w) (ArC−ArC), 1458 (w), 1410 (w), 1363 (m) (Cl−ArC−ArC−Cl), 1340 (m) (Cl−ArC−ArC−Cl), 1295 (m) (Cl−ArC−ArC−Cl), 1259 (m) (Cl−ArC−ArC−Cl), 1139 (m), 968 (m), 949 (m), 871 (w), 859 (w), 807 (s) (C-Cl), 712 (w), 707 (w), 690 (w), 670 (m), 649 (m), 640 (w), 626 (w), 616 (w), 584 (w), 574 (w), 565 (w), 550 (w), 539 (sh, w), 527 (m), 520 (m), 510 (w); **UV-Vis** ($CHCl_3$): λ (nm) (ξ, M^{-1} cm^{-1})□309 (46231), 339 (78308), 358 (126846), 376 (133423), 401 (75038), 434 (43385), 473 (18269).

4. Additional electrochemical data

Scheme S3. *Chemical structure of compound* ***2-R*** *together with reference compounds* ***1-R*** *and (****1-R-Br****). Dashed rectangles highlight the stilbene analogue core (red) and the perchlorotriphenylmethyl (●PTM) radical moiety (blue).*

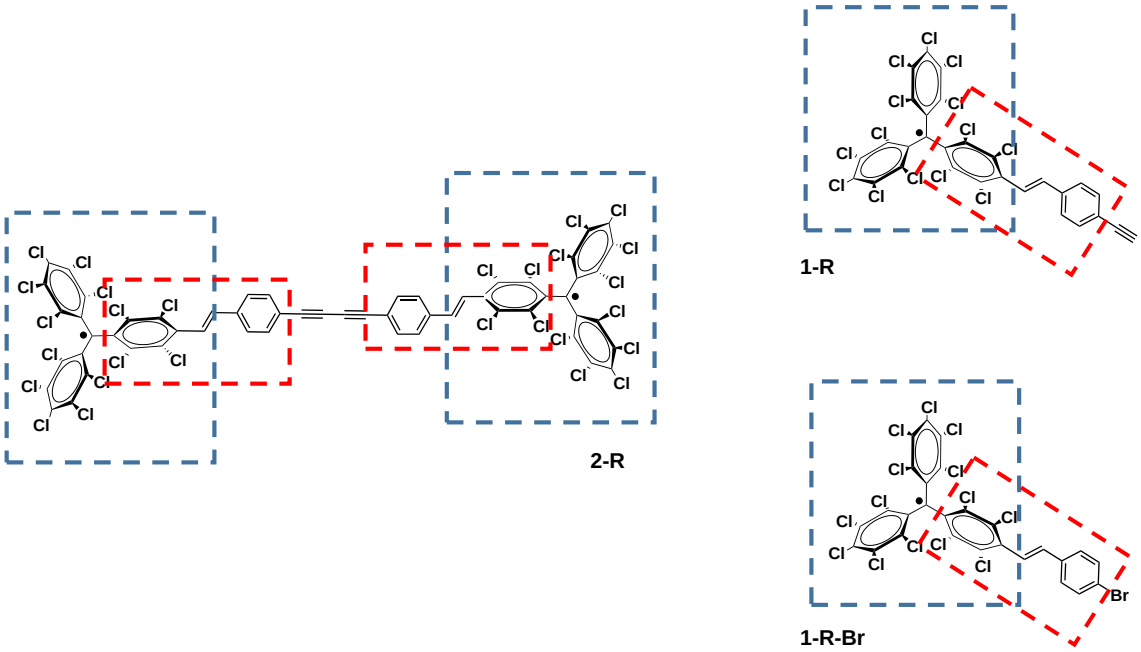

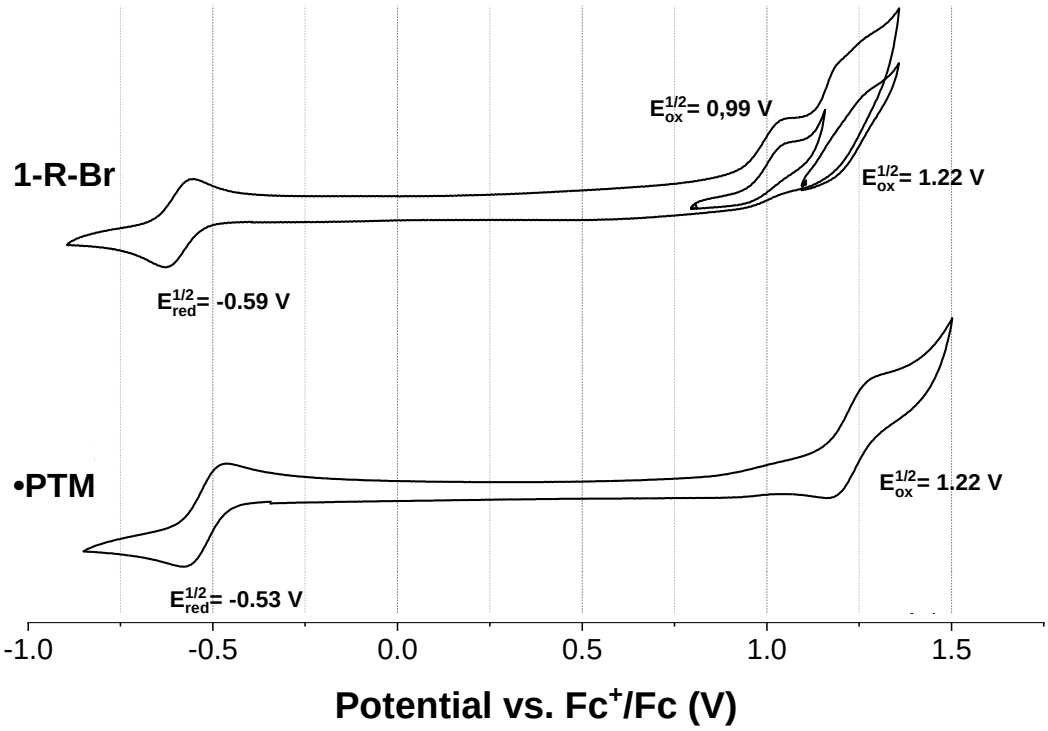

Figure S1. *Cyclic voltammograms recorded for 10^{-4} M solutions of ●PTM and* ***1-R-Br*** *recorded at room temperature in 0.2 M n-Bu_4PF_6 / DCM as electrolyte under Ar atmosphere. Counter and working electrodes: Pt wires. Pseudo-reference: Ag wire. Internal reference: Ferrocene.*

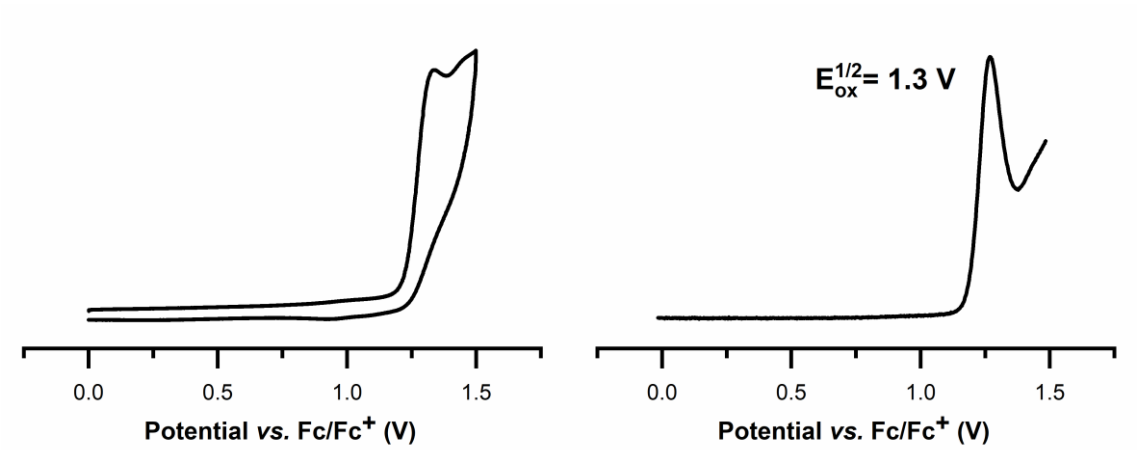

Figure S2. *CV (left) and DPV (right) of* ***2-H*** *recorded at room temperature in 0.2 M n-Bu_4PF_6 / DCM as electrolyte. Counter and working electrodes: Pt wires. Pseudo-reference: Ag wire. Internal reference: Ferrocene.*

5. Mixed-valence (MV) radical-anion formation

2-R-Red, PTM(radical)-bridge-PTM(anion), was freshly prepared prior to its ESR study. To this end, an heterogeneous reduction was carried out with metallic copper pieces immersed in a **2-R** solution (~6–7 × 10^{-5} M is the optimum concentration).[2] The Cu pieces can be easily and rapidly removed from the solution at any moment, thus providing an excellent way to halt the reaction at the desired point. However, the heterogeneity of the reaction required the presence of an electrolytic medium to work properly. Since it is known that bulky counterions, such as PPh_4^+, stabilize the PTM anions,[3] tetraphenylphosphonium bromide (PPh_4Br, 0.1 M) was chosen for the study. The reaction was followed by UV-Vis spectroscopy **(Figure S3a**) and stopped after 33 minutes, when the dianion species was not completely formed.

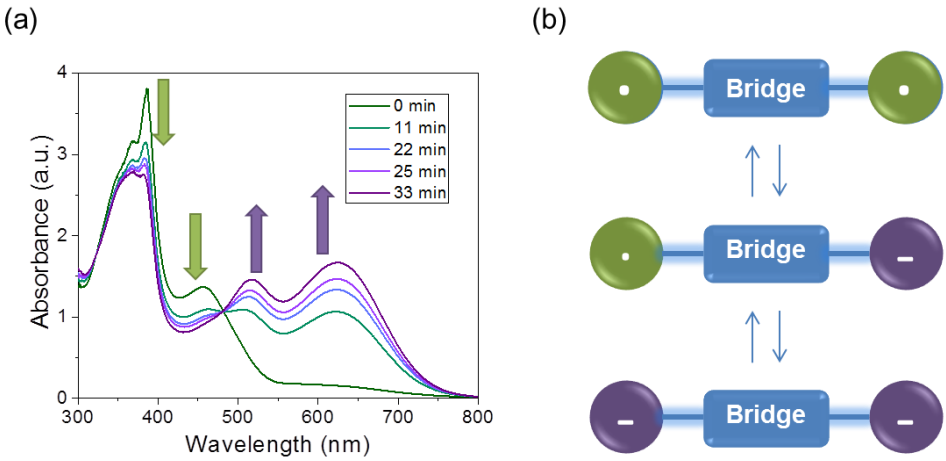

Figure S3. *(a) Spectral changes in the UV-Vis measurements upon diradical* ***2-R*** *chemical reduction. The bands corresponding to the PTM radical (~385 and ~450 nm, green arrows) diminish, whereas the anionic ones (~530 and ~620 nm, purple arrows) increase. (b) Schematics of the comproportionation equilibrium between the diradical (top), the dianion (bottom) and the MV compound (center).*

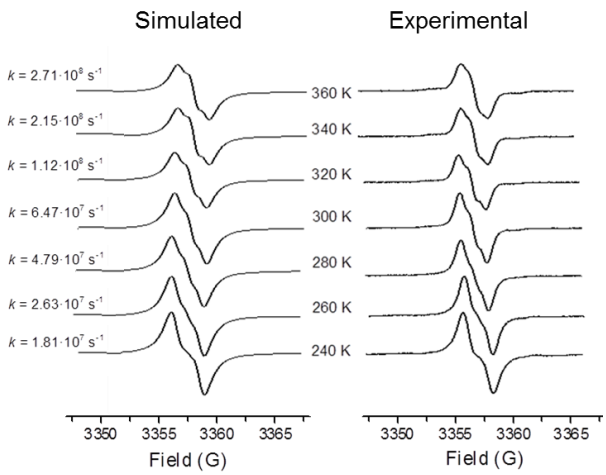

Figure S4. *Temperature-dependent evolution of the ESR spectra of* ***2-R-Red*** *in saturated PPh_4Br/oDCB solution (right), together with the simulated ESR spectra (left) with the different spin/charge exchange rates (k_{ET}) quoted.*

The thermodynamic parametres in DCM and in oDCB were determined from the intramolecular electron transfer (IET) rate constants (k_{ET}) through Arrhenius plots (log(k_{ET}) vs 1/T) of the k_{ET} values obtained from the variable-temperature ESR spectra (**Figure S4** and **Figure S5**). All the thermodynamic parameters were calculated considering a confidence interval of 95% and are detailed in the following table:

	ΔH* (cal mol^{-1})	ΔS* (cal mol^{-1} K^{-1})	ΔG*$_{298\ K}$ (cal mol^{-1})
2-R-Red in CH_2Cl_2	2.5 ± 0.3 ·10^3	-16 ± 1	7.3 ± 0.6 ·10^3
2-R-Red in oDCB	3.4 ± 0.3 ·10^3	-10.9 ± 0.9	6.7 ± 0.5 ·10^3

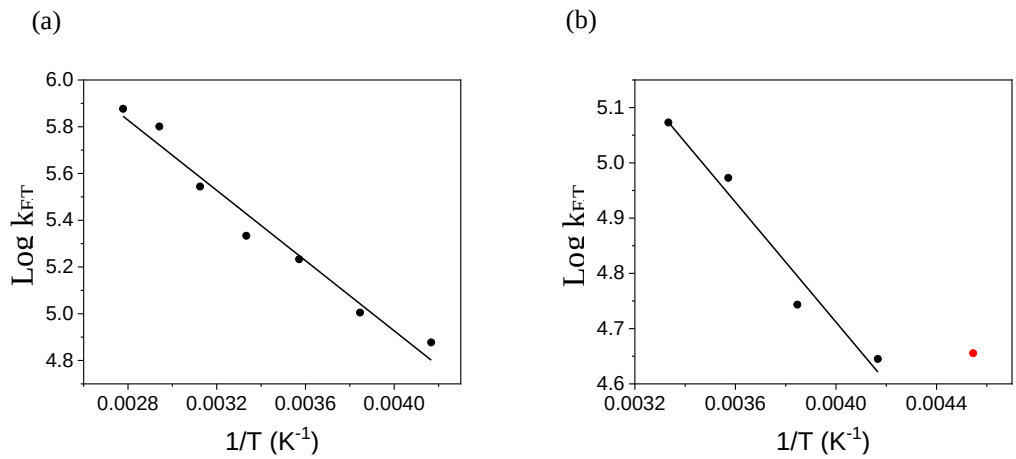

Figure S5. *Arrhenius plot of the intramolecular electron transfer (IET) rate constants (k_{ET}) for* ***2-R-Red*** *in a) oDCB and b) DCM. The point corresponding to the experiment at 220 K (red dot) was ruled out because it appeared far from the linearity.*

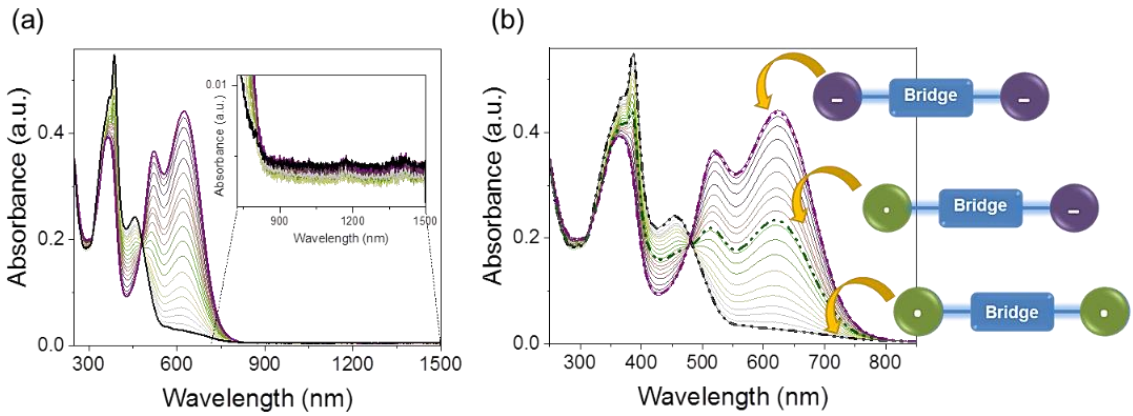

Figure S6. *(a) UV-Vis-NIR absorption spectra following the complete electrochemical reduction of* ***2-R*** *to the dianion form. No Intervalence charge transfer (IV-CT) band is observed in the NIR region (inset). (b) Zoom into the UV-Vis region from (a). The dashed spectra correspond to the three species involved in the comproportionation equilibrium.*

6. Spectroelectrochemical analysis of cationic species

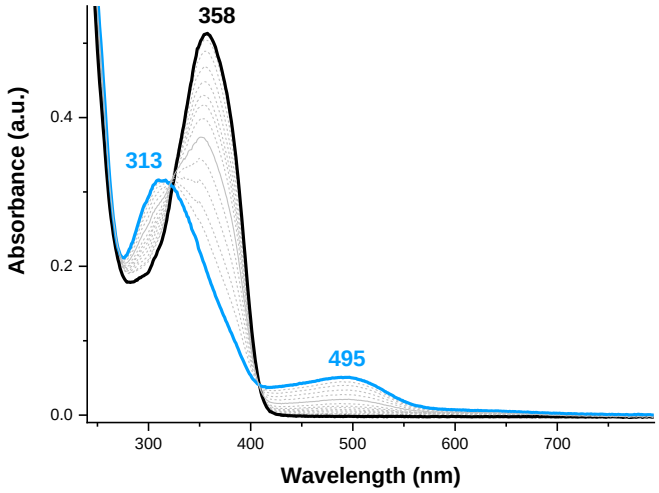

Figure S7. *UV-Vis absorption electronic spectra for the electrochemical oxidation of* ***2-H*** *from neutral (black solid line) to its oxidized species,* ***2-H-Ox*** *(blue solid line), and grey dashed lines for transient species.*

7. Chemical oxidation of 2-R

Scheme S4. *Proposed oxidation processes for **1-R** and **2-R** with a common dimerization step after the electron removal (i).*

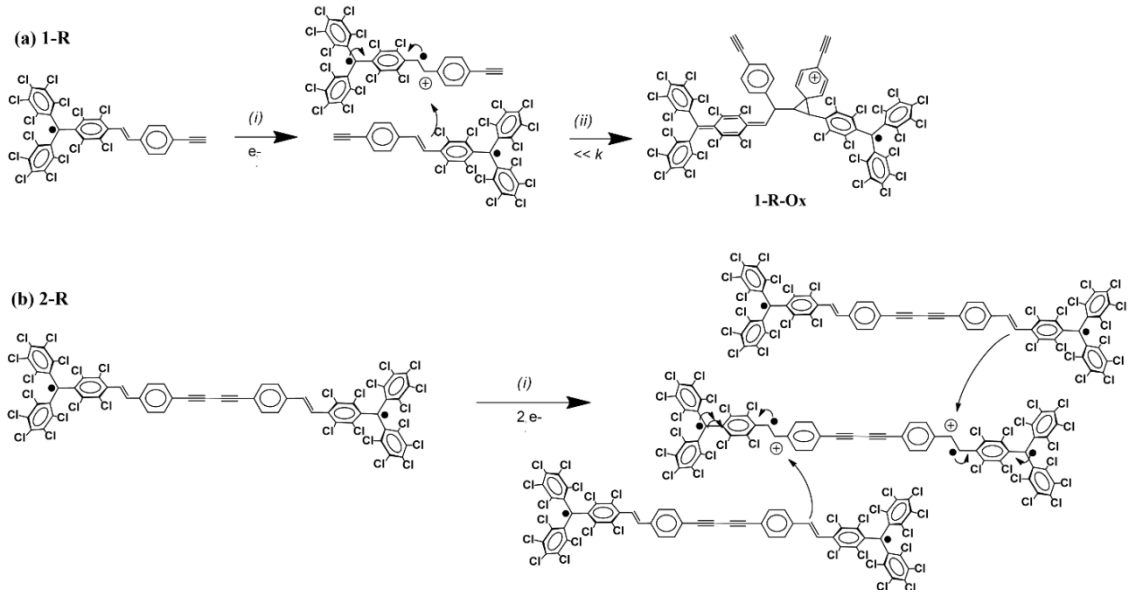

The generation of **2-R-Ox** was achieved by chemical means using nitrosonium tetrafluoroborate ($NOBF_4$). A **2-R** solution in dry DCM (*ca.* 6×10^{-4} M) was prepared under inert atmosphere and red light. On the other hand, a solution of moisture sensitive $NOBF_4$ was prepared inside a glove box with dry ACN. Up to 15 equivalents of $NOBF_4$ were stepwise added to the solution of **2-R** for the full achievement of the **2-R-Ox** species. The reaction was monitored *in-situ* by UV-Vis spectroscopy, and a UV-Vis spectrum equivalent to that recorded during the spectroelectrochemical measurements was obtained. Additionally, a clear color change from the initial dark green to red **(Figure S8**) was observed after the completion of the reaction in 5–10 minutes. **2-R-Ox** was then isolated as a red solid after the removal, under vacuum, of the solvent.

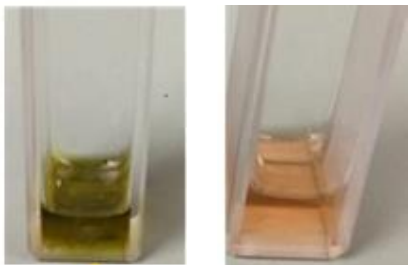

Figure S8. *Color change observed upon chemical oxidation of **2-R** with $NOBF_4$, going from dark greenish to redish.*

8. ESR measurements of 1-R-Ox and 2-R-Ox

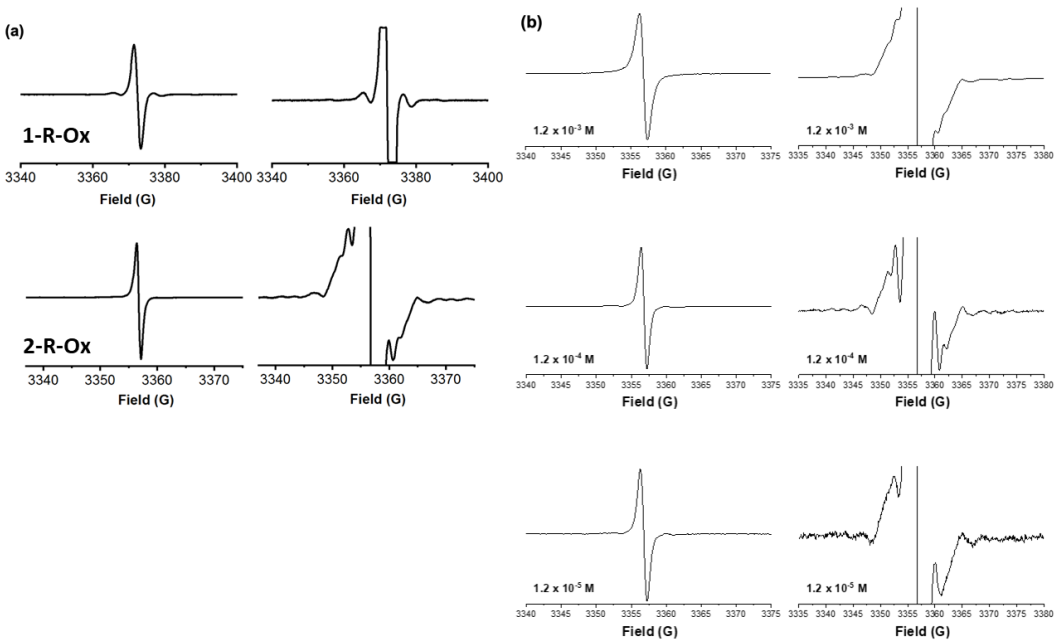

Figure S9. a) *ESR spectra of* ***1-R-Ox*** *and* ***2-R-Ox*** *in solution at 9x10^{-4}M (g = 2.0031) recorded at room temperature and* ***b)*** *ESR spectra of* ***2-R-Ox*** *at different concentrations (from 1.2 × 10^{-3} to 1.2 × 10^{-5} M). For (a) and (b): (left) in normal and (right) at higher gain acquisition conditions.*

From the spectrum acquired at higher gain for the **2-R-Ox** at 9x10^{-4}M in DCM (**Figure S9a**), weak signals derived from electron-^{13}C nuclei couplings at 29.5 G (assigned to the coupling with the α-C,) and 9.9 G (coupling with aromatic ^{13}C atoms of the chlorinated phenyl rings) were observed. The coupling constants with ^{13}C at 6.5 and 17.0 G, could be attributed to intermolecular magnetic interactions in **2-R-Ox**. In a molecule with interacting radicals, those values would be related to the coupling constants with the *α*-C and the aromatic C, respectively. It is worth mentioning that these constants, in the absence of radical coupling, would be ~12 and ~30 G, respectively, *i.e.*, twice the observed ones. Thus, the formation of aggregates at these experimental conditions was thought. Unfortunately, the half-field peak could not be directly checked at lower concentrations because of experimental limitations (a concentration close to 10^{-3}M is required for its detection). However, as depicted in **Figure S9b**, ESR spectra of **2-R-Ox** at different concentrations were taken to check the possible influence of intermolecular interactions and the same spectral shape was obtained in all cases, ruling out this hypothesis. According to these results, an alternative explanation for the observation of the half-field signal might be an intramolecular radical interaction arising from a covalent dimer rather than a supramolecular aggregate, since: (i) the dimerization of radical-cations of stilbene derivatives with their neutral analogues is already known;[4,5] and (ii) the theoretical calculations performed for **1-R** support this hypothesis (following section).

9. DFT calculations for 1-R-Ox

Theoretical calculations were performed using the density functional theory (DFT) approach through the Gaussian-16.A02 suite of programs.[6] Molecular geometries, natural orbitals, and spin densities were visualized through the Chemcraft software.[7] The minimum-energy structures of the hypothetical adduct of **1-R-Ox** were obtained at the M06-2X/6-31G** level of theory[8–10] including the Grimme's D3 dispersion correction.[11,12] Solvent effects were incorporated by means of the SMD model with dichloromethane as solvent.[13] The first structure analysed for **1-R-Ox**, named as structure **A**, corresponds to two molecules of **1-R** (**[1-R]$_2^{\bullet+}$** dimer) bonded through two bridging ethylene carbon atoms to form a □-type adduct (**Figure S10**). Structure **A** can be visualized as a cationic dimer where the radical spreads all over one monomer (both the PTM and the phenylacetylene (PA) units), whereas the other moiety adopts a quinoid form. Structure **A** was therefore calculated as a radical (doublet, 2S+1 = 2) with a positive charge (+1e). The carbon-carbon bond distances calculated for structure **A** are displayed in **Figure S10** (bottom) and confirm the different structure shown by the two PTM moieties.

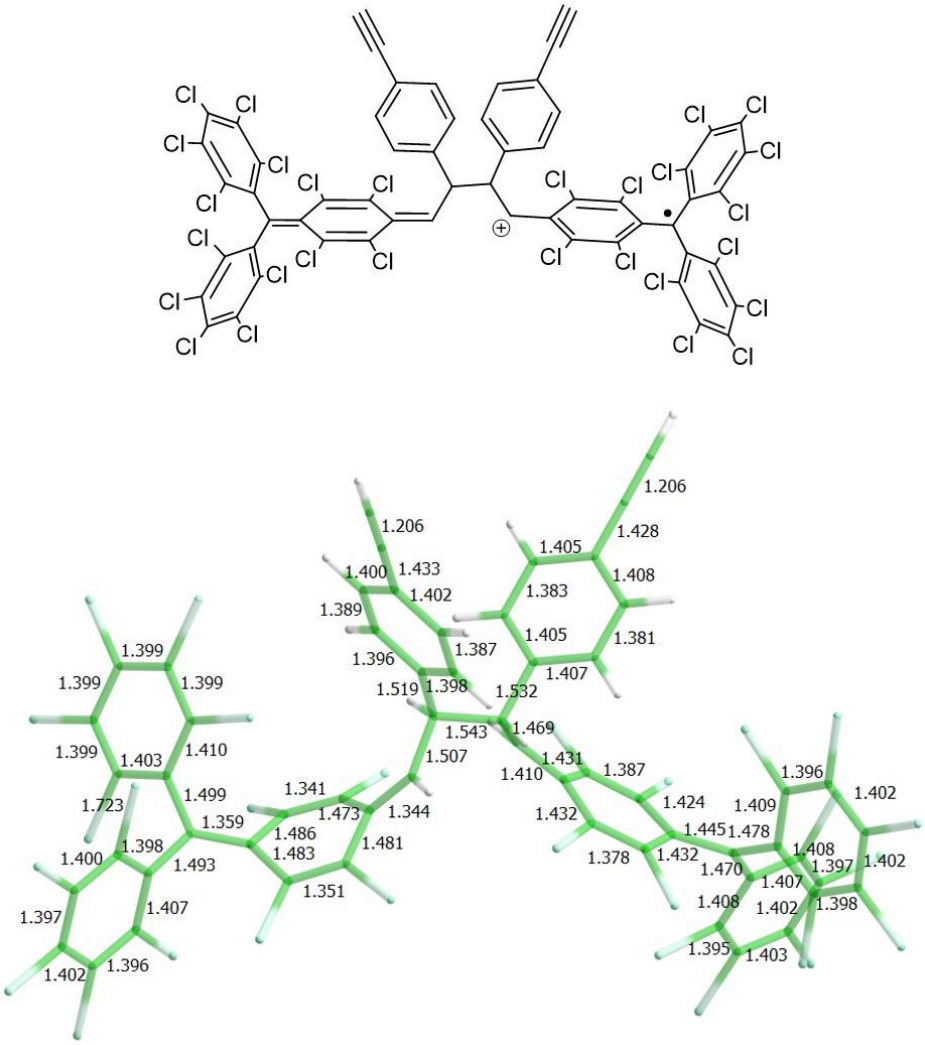

Figure S10**. Chemical structure (top) and carbon-carbon bond distances (in Å, bottom) calculated at the M06-2X-D3/6-31G** level for structure **A** of the hypothetical **[1-R]$_2^{\bullet+}$** adduct of **1-R-Ox.

The Mulliken atomic charges and spin densities computed for structure **A** (**Figure S11**) confirm the localization of the positive charge and the unpaired electron on one of the two PTM-PA moieties of the **[1-R]$_2^{\bullet+}$** cation. In particular, approximately half of the positive charge is accumulated on the PTM unit (+0.48e), whereas the other half is on the PA moiety (+0.41e). The unpaired-electron spin density mainly spreads over the PTM unit and has a large contribution on the vinylene carbon bearing a hydrogen atom. This would lead to a splitting of the ESR signal, contradicting the experimental data recorded for **1-R-Ox**.

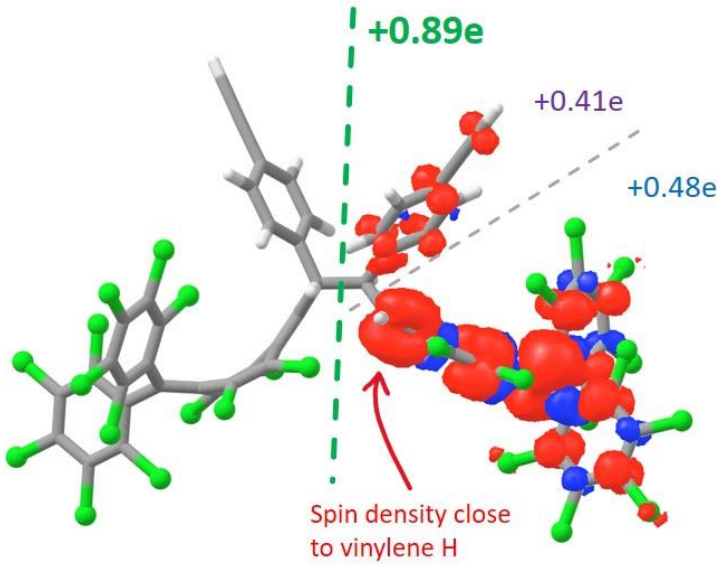

Figure S11. *Accumulated Mulliken charges (in e) and representation of the Mulliken spin density (isovalue = 0.001 a.u.) calculated at the M06-2X-D3/6-31G** level for structure **A** of **[1-R]$_2^{\bullet+}$**.*

Frequency M06-2X/6-31G** calculations indicate that structure **A** possesses a small imaginary frequency and therefore corresponds to a first-order transition state. The displacement vectors associated to the imaginary frequency mainly involve the twisting of one PA unit (**Figure S12**) and lead to the formation of a cyclopropane ring giving rise to a new structure, named as structure **B**, for the **[1-R]$_2^{\bullet+}$** cation (**Figure S13**). Structure **B** was computed at the M06-2X-D3/6-31G** level as a radical (doublet, 2S+1 = 2) with a positive charge (+1e) and shows no imaginary frequency. It therefore corresponds to a true energy minimum. Structure **B** was calculated to be 14.5 kcal mol^{-1} more stable than structure **A**. This energy difference corresponds to the Gibbs free energy difference including solvent effects (PCM model, dichloromethane) and zero-point energy and thermal corrections using the quasi rigid-rotor harmonic oscillator (quasi-RRHO) approach developed by Grimme.[14] The optimized carbon-carbon bond lengths (**Figure S13**) indicate that structure **B** can be visualized as a dimer constituted by a quinoid PTM moiety and a more aromatic PTM moiety bearing the unpaired electron with the positive charge mainly localized on the adjacent PA unit. The Mulliken atomic charges and spin densities calculated for structure **B** confirm the localization of the charge on one PA unit and the unpaired electron on the vicinal PTM moiety (**Figure S14**). The PTM radical is therefore electronically disconnected from the rest of the molecular system due to the cyclopropane ring formation. It is to be emphasized that the vinylene carbon forming the cyclopropane ring now shows no contribution to the spin density in good agreement with the experimental ESR spectrum recorded for **1-R-Ox**, which presents no splitting of the ESR signal due to the spin coupling with any hydrogen atom (**Figure 3**, main text).

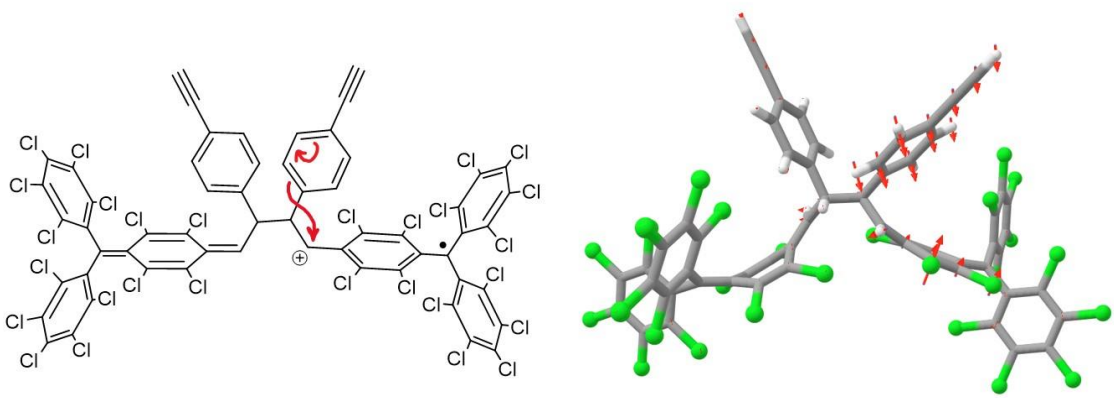

Figure S12. *Chemical sketch (left) and imaginary frequency (30i cm^{-1}, right) that connect structure **A** into the more stable cyclopropane ring-containing structure **B** of the **[1-R]$_2^{\bullet+}$** adduct.*

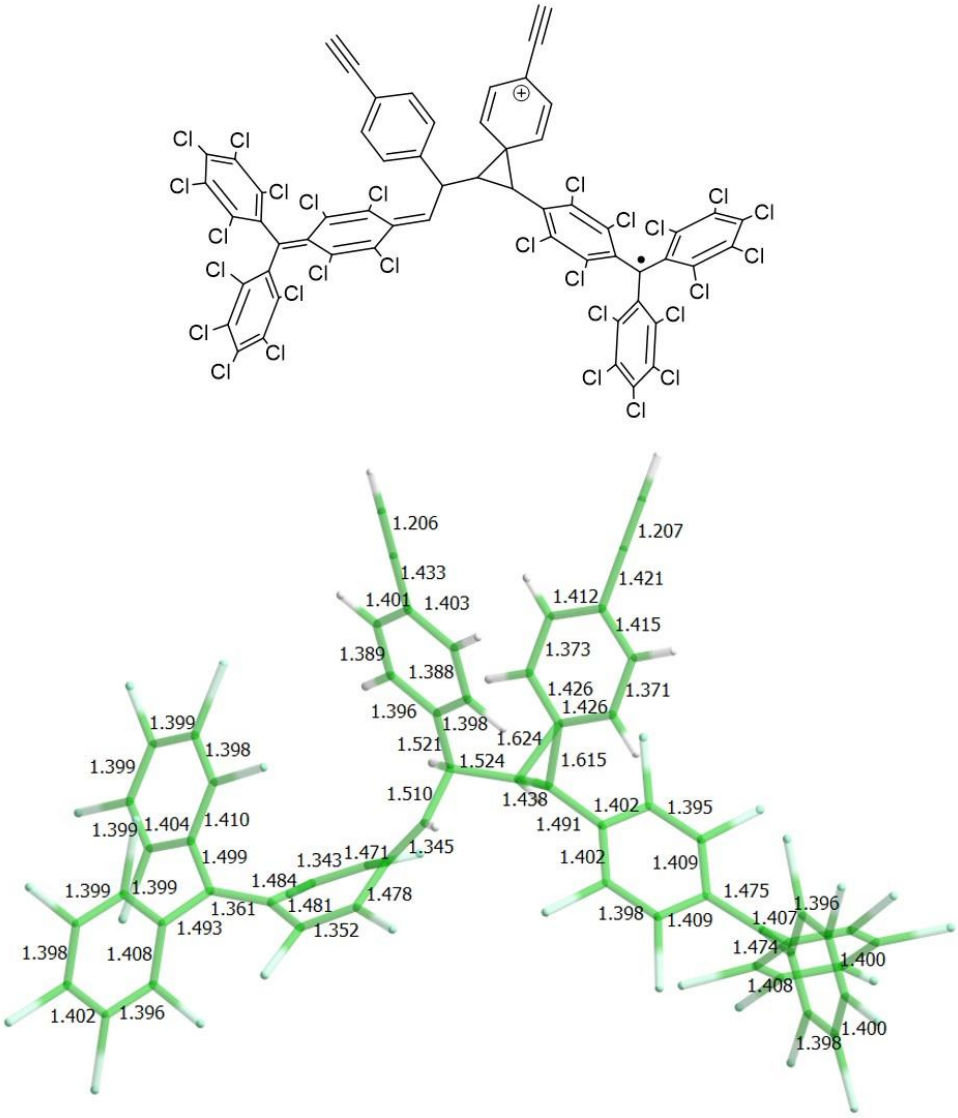

Figure S13*. Chemical structure (top) and carbon-carbon bond distances (in Å, bottom) calculated at the M06-2X-D3/6-31G** level for structure* ***B*** *of the* ***[1-R]₂•⁺*** *adduct of the oxidized species of* ***1-R****.*

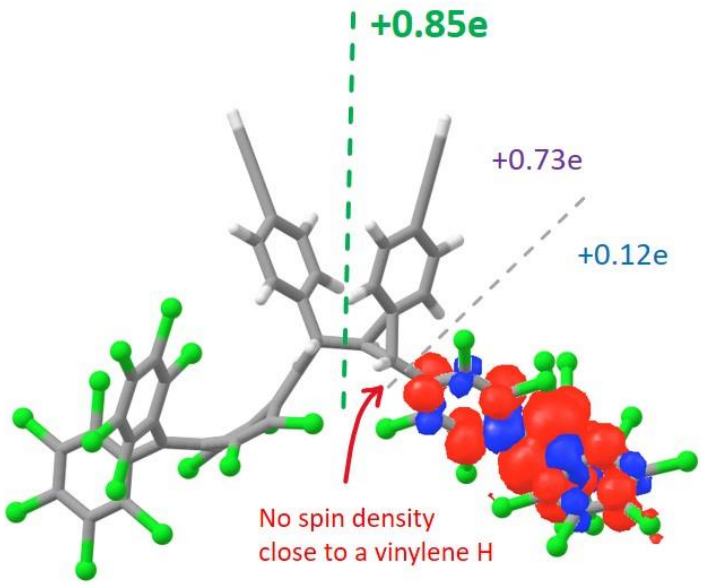

Figure S14. *Accumulated Mulliken charges (in e) and representation of the Mulliken spin density (isovalue = 0.001 a.u.) calculated at the M06-2X-D3/6-31G** level for structure* ***B*** *of* ***[1-R]$_2^{\bullet+}$****.*

The time-dependent DFT (TDDFT) approach[15,16] was used to compute the electronic absorption spectra of the hypothesized structures **A** and **B** of **[1-R]$_2^{\bullet+}$**. The lowest-lying singlet excited states were computed at the CAM-B3LYP/6-31G** level of theory[17] by using the minimum-energy geometries previously calculated at the M062X-D3/6-31G** level. The simulated absorption spectra (**Figure S15**) were obtained by convoluting the excitation energies to Gaussian functions of full-width-at-half-maximum (FWHM) of 0.2 eV. The nature of the main electronic transitions was analyzed by computing the natural transition orbitals (NTOs) at the same level of theory. The absorption spectrum of the cation dimer with a cyclopropane unit (structure **B**) better fits the experimental absorption spectrum of the oxidized species **[1-R]$_2^{\bullet+}$** (compare **Figure 2c** (main text) and **Figure S15**). The analysis of the electronic excitations leading to the absorption spectrum of structure **B** indicates that the low-lying transitions in **[1-R]$_2^{\bullet+}$** are charge-transfer (CT) excitations from the quinoid PTM environment and the adjacent neutral PA unit to the positively charged PA unit (**Figure S16**). The intense peak predicted just below 400 nm, in good accord with the experimental spectra (**Figure 2c,** main text), is described by local excitations over the PTM units similarly to that obtained for the isolated ●PTM (**Figure 2f**). Due to conjugation breaking upon cyclopropane formation, signatures above 400 nm involving the PTM+PA moiety in **1-R** disappear as experimentally observed (inset **Figure S16**).

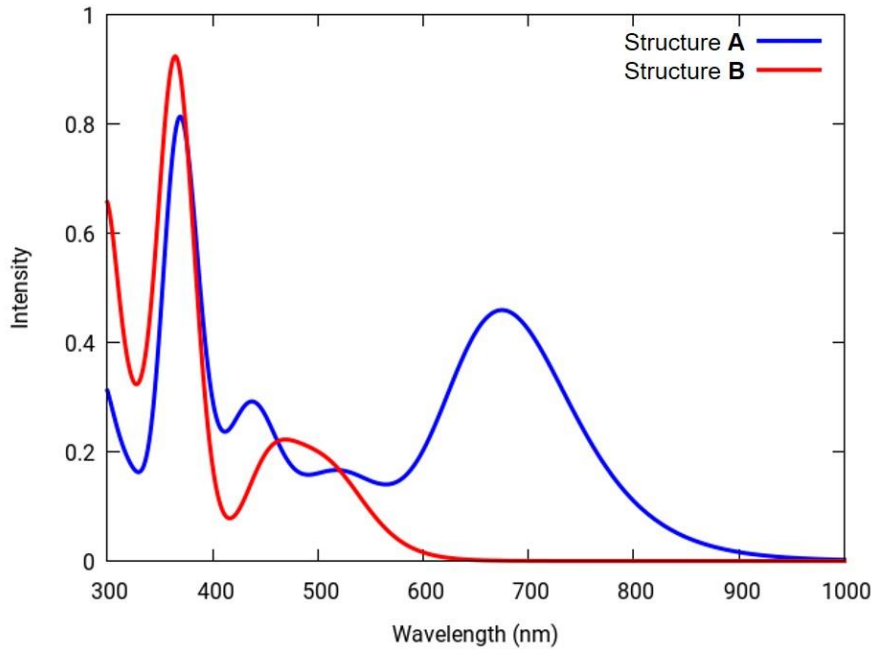

Figure S15. *Simulated TD-DFT absorption spectra calculated at the CAM-B3LYP/6-31G** level for structures **A** and **B** hypothesized for the cation dimer* ***[1-R]$_2^{\bullet+}$****.*

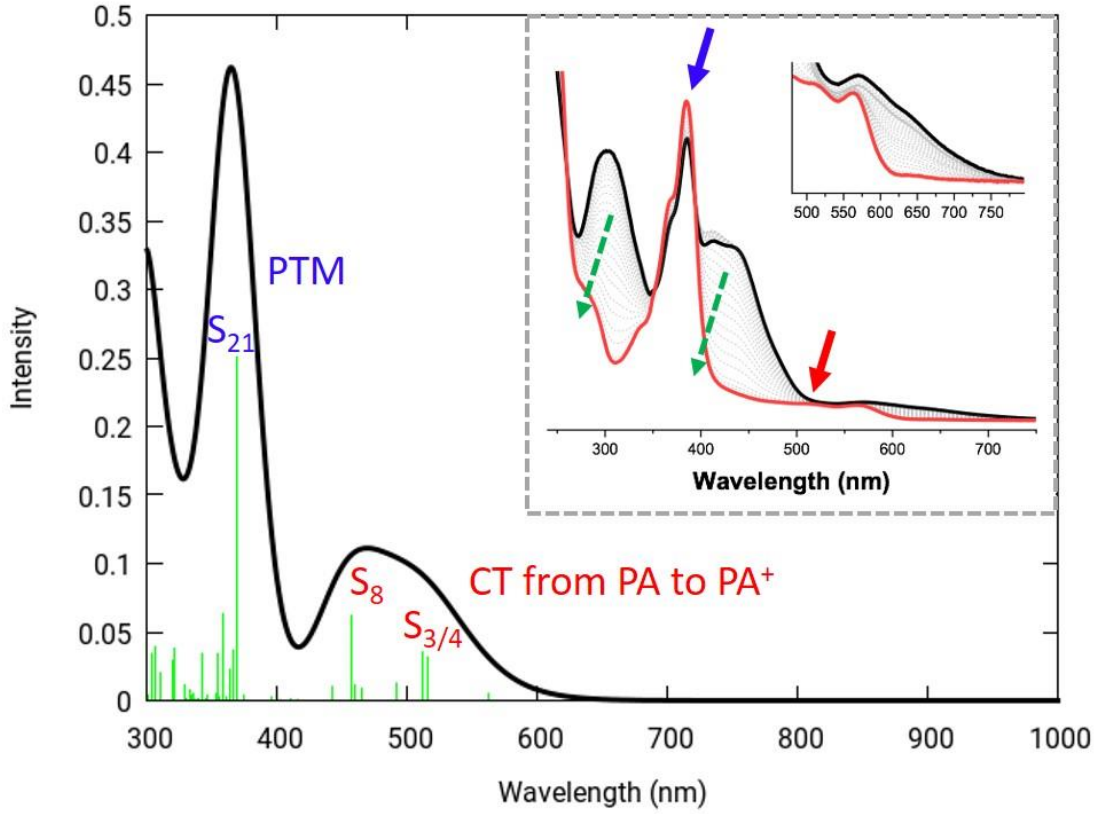

Figure S16. *TD-DFT CAM-B3LYP/6-31G** absorption spectrum predicted for the cyclopropane ring-containing structure **B** of* ***[1-R]$_2^{\bullet+}$****, together with the sticks (green) indicating the positions, oscillatory strengths, and nature of the calculated electronic transitions (see Figure S17 for the NTOs giving rise to the transitions). Inset: experimental UV-Vis electronic absorption spectra of* ***1-R*** *obtained during its potentiostatic oxidation. Black solid line: neutral species. Red solid line: radical cation. Dashed lines correspond to transition spectra.*

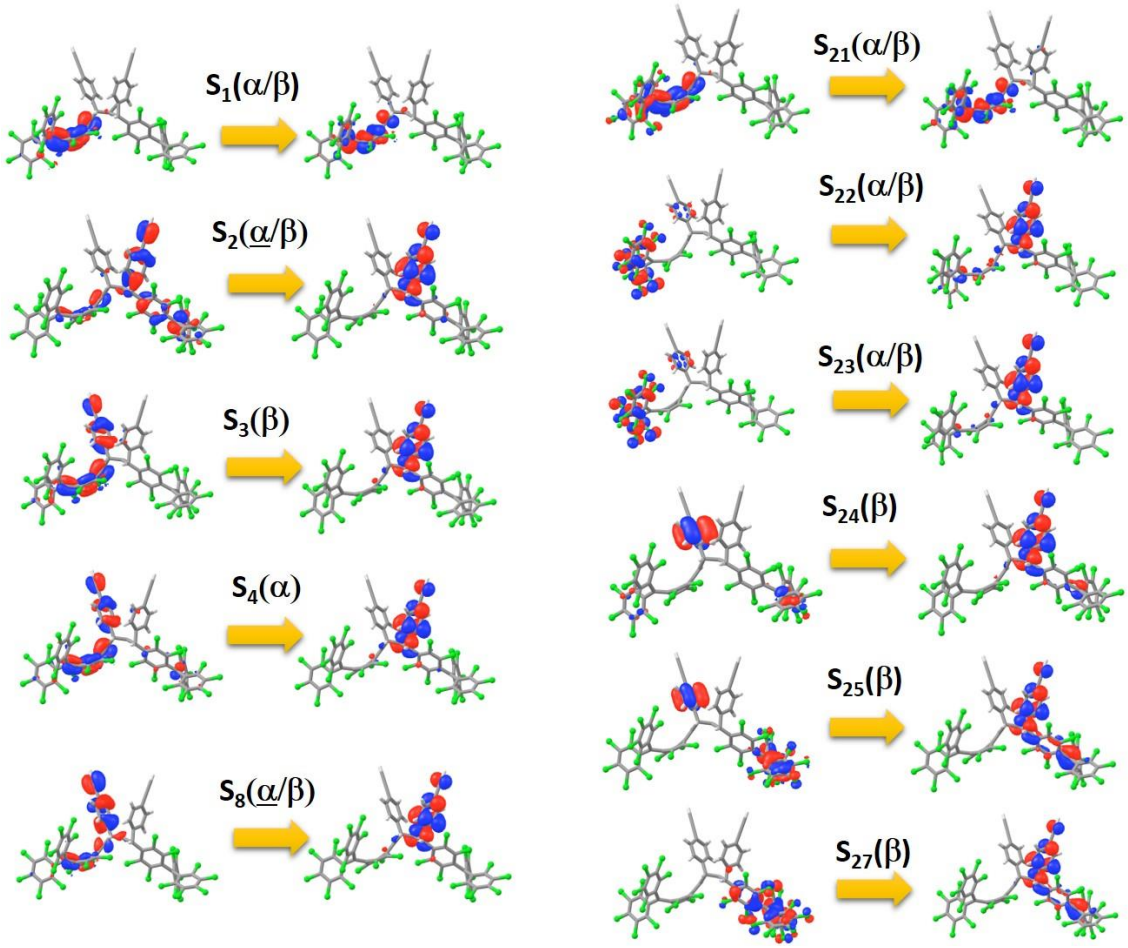

Figure S17. *Natural transition orbitals (NTOs) mainly involved in the description of the electronic excitations calculated for structure* ***B*** *of* ***[1-R]$_2^{\bullet+}$***.

10. Mass spectrometry measurements for 2-R-Ox

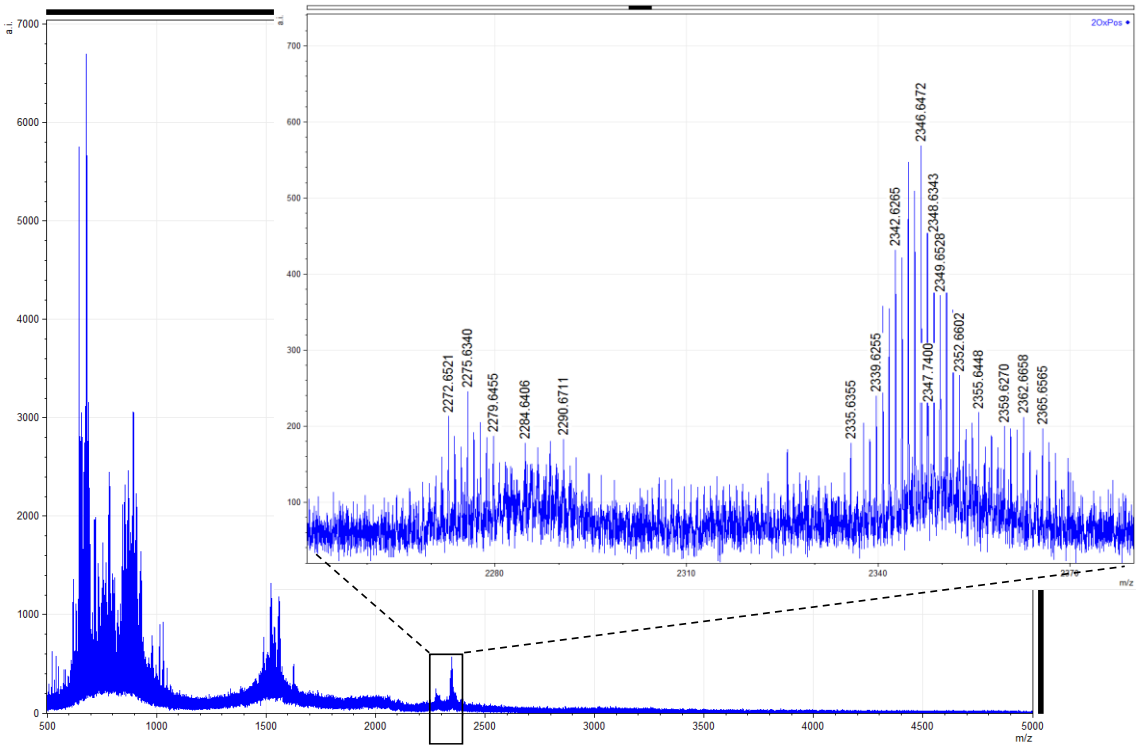

Figure S18. *MALDI-ToF spectrum for* ***2-R-Ox****.*

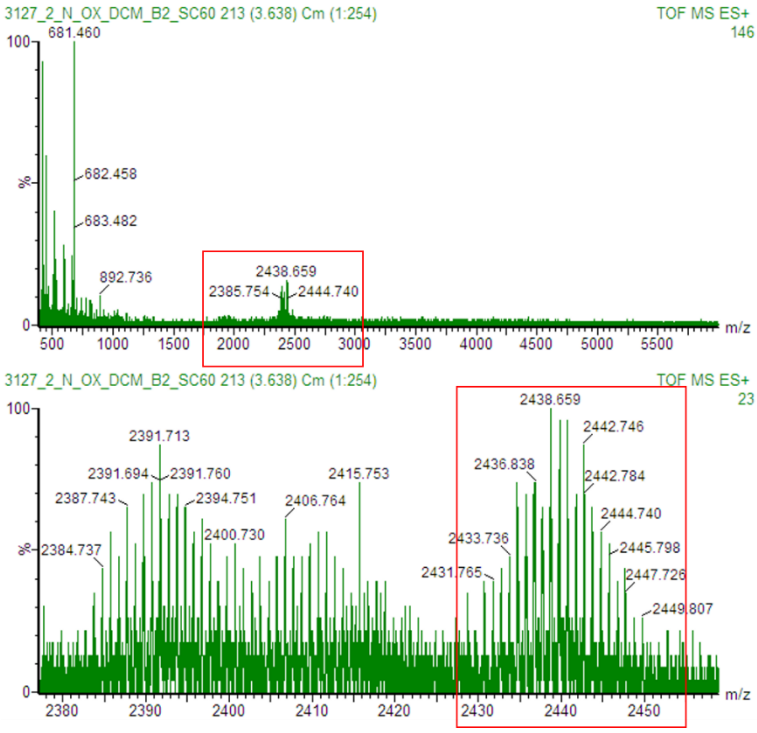

Figure S19. *ES+ ToF MS spectrum for* ***2-R-Ox.***

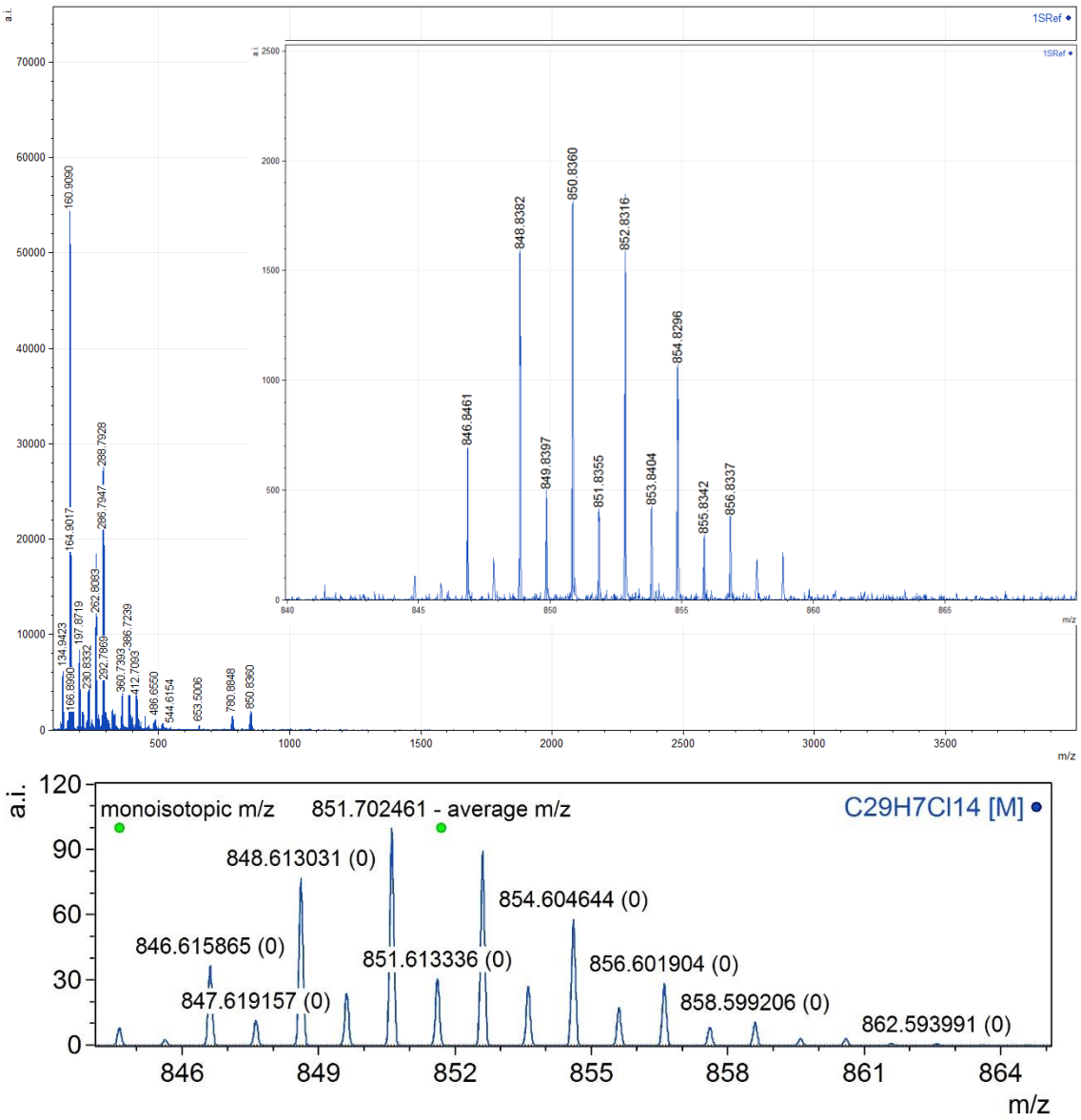

Figure S20. *Experimental MALDI-ToF spectrum of compound* ***1-R*** *(top, m/z = 850.83 [M-H]⁻) together with its theoretical isotope mass distribution (bottom, m/z = 851.70 [M]. $C_{29}H_7Cl_{14}$).*

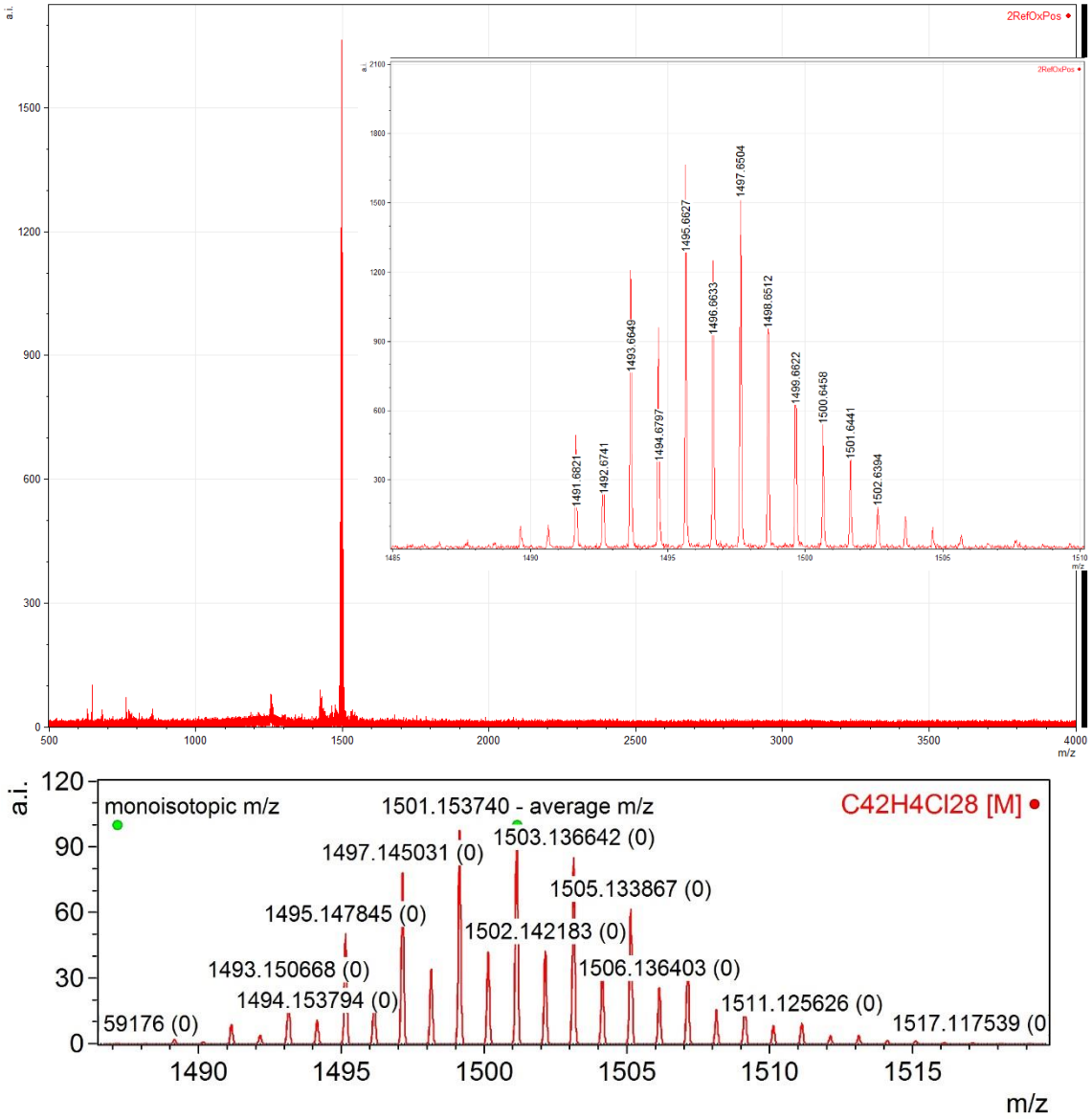

Figure S21. *Experimental MALDI-ToF spectrum of compound* ***[1-R]$_2^{\bullet+}$*** *(top, base peak: m/z = 1497.65) together with the simulated spectrum of a fragment of the dimer (bottom, m/z= 1501.15. $C_{42}H_4Cl_{28}$).*

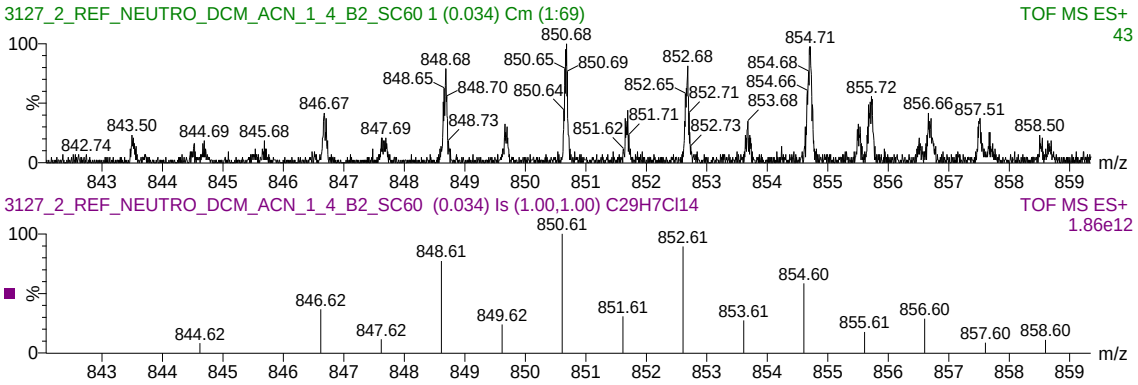

Figure S22. *Experimental ES+ ToF MS spectrum for* ***1-R*** *(top, m/z = 850.68 [M-H]⁻) recorded in an DCM:ACN (1:4) solution, together with its theoretical isotope mass distribution (bottom, m/z=850.61. $C_{29}H_7Cl_{14}$).*

11. ANEX I: ^{1}H-NMR, ^{13}C-NMR, FT-IR and LDI-ToF data

(a) Compound 2-H

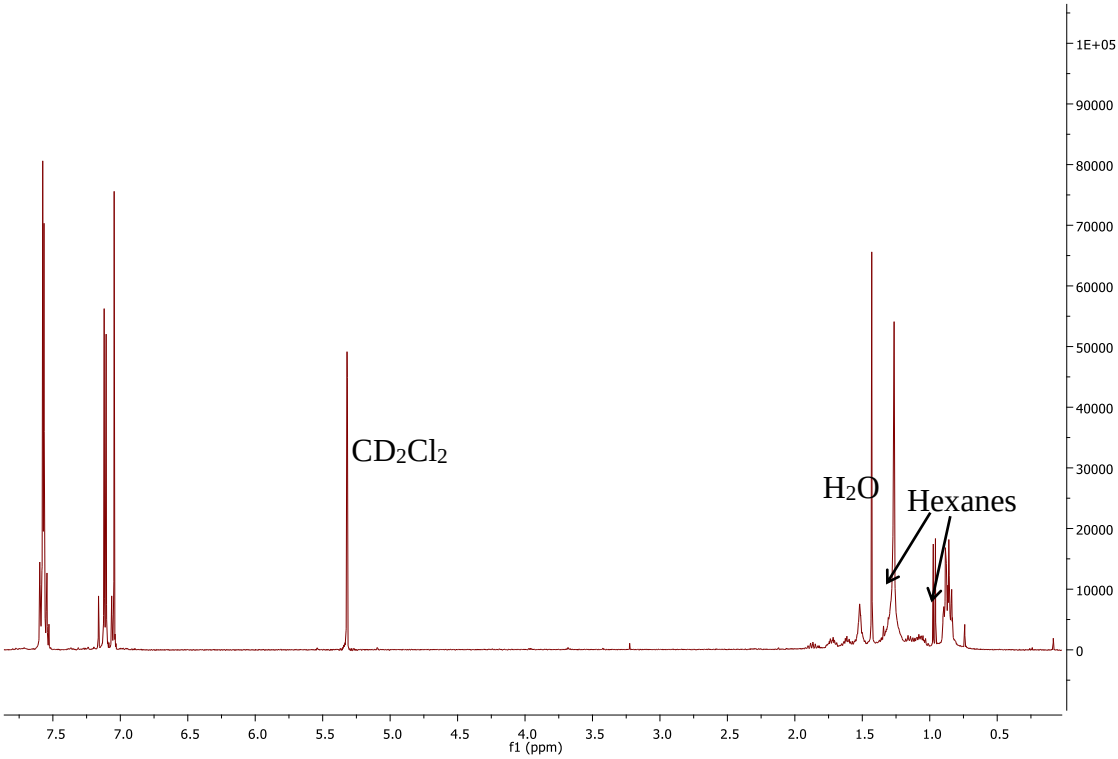

Figure S23. *^{1}H-NMR spectrum of compound **2-H** in CD_2Cl_2.*

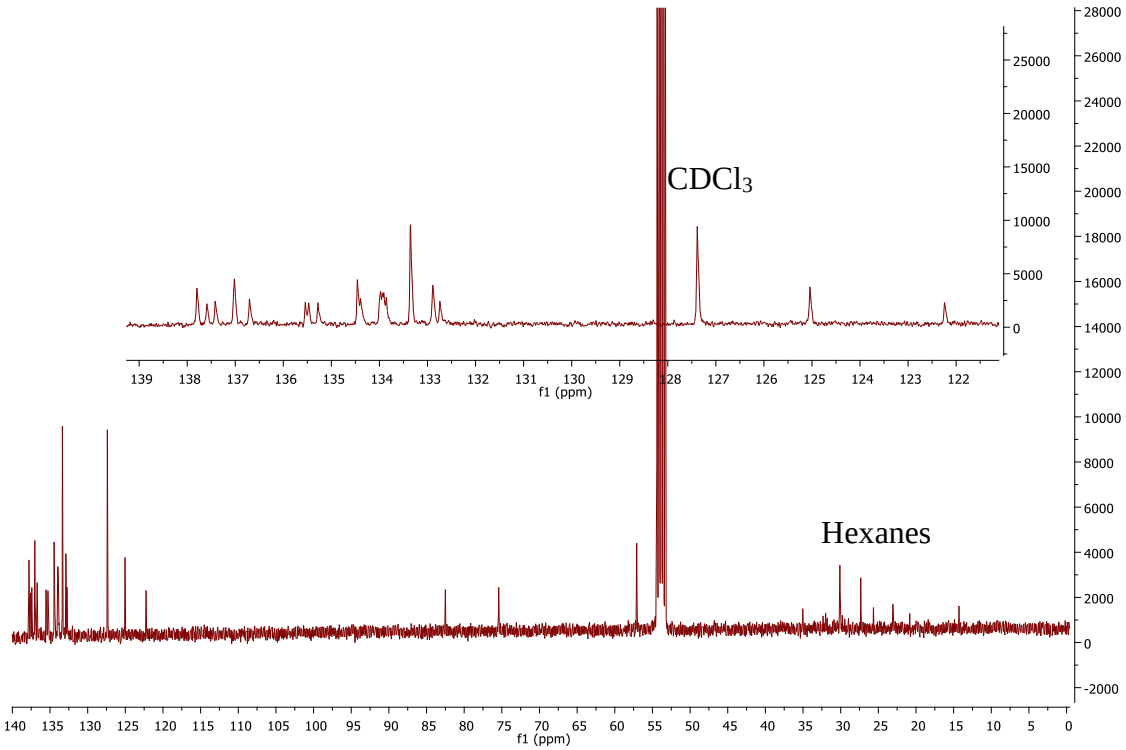

Figure S24. *^{13}C-NMR spectrum of compound **2-H** in $CDCl_3$.*

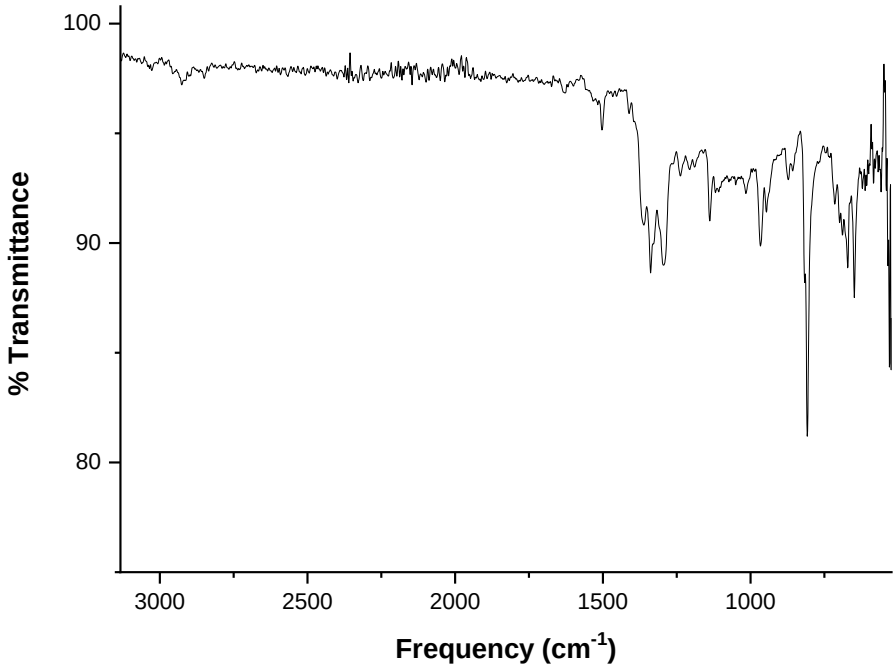

Figure S25. *FT-IR spectrum of compound* ***2-H*** *in powder.*

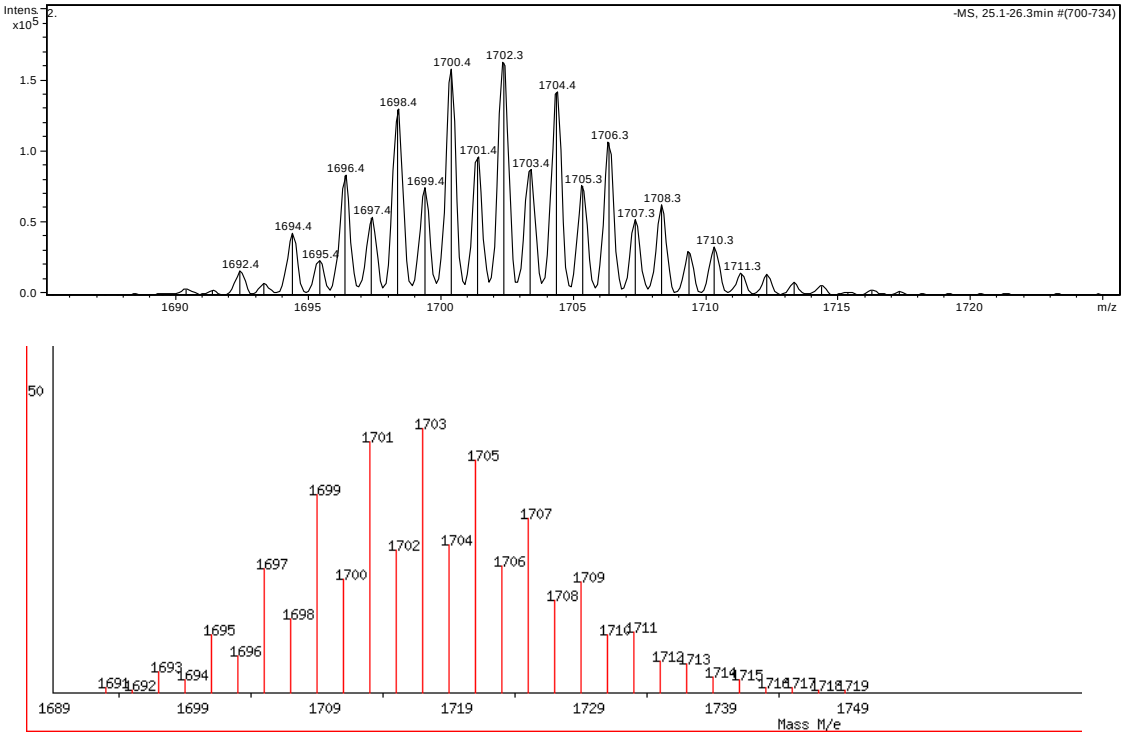

Figure S26. *Experimental (top) and simulated (bottom) LDI-ToF spectra of compound* ***2-H****.*

(b) Compound 2-R

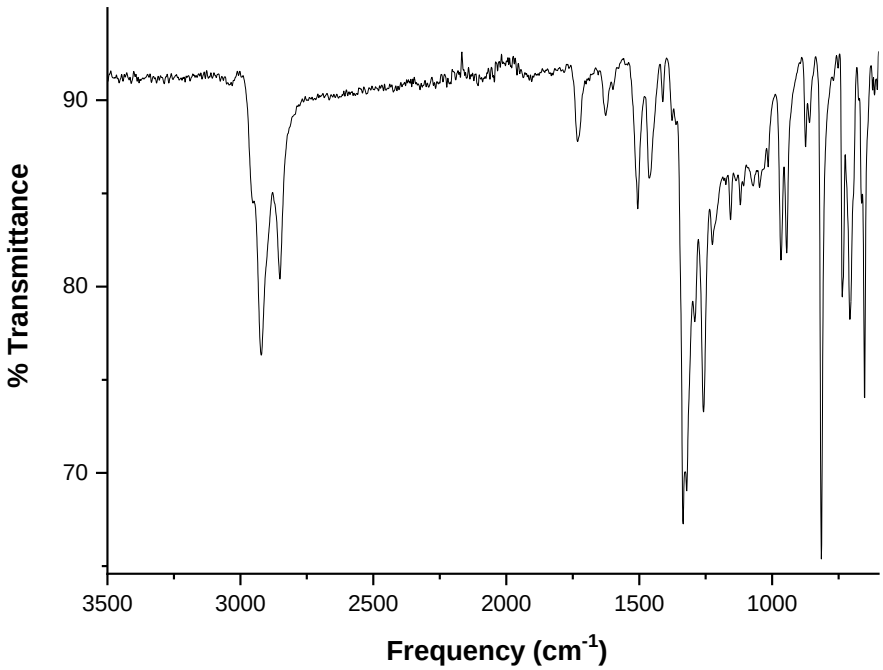

Figure S27. *FT-IR spectrum of compound* ***2-R*** *in powder.*

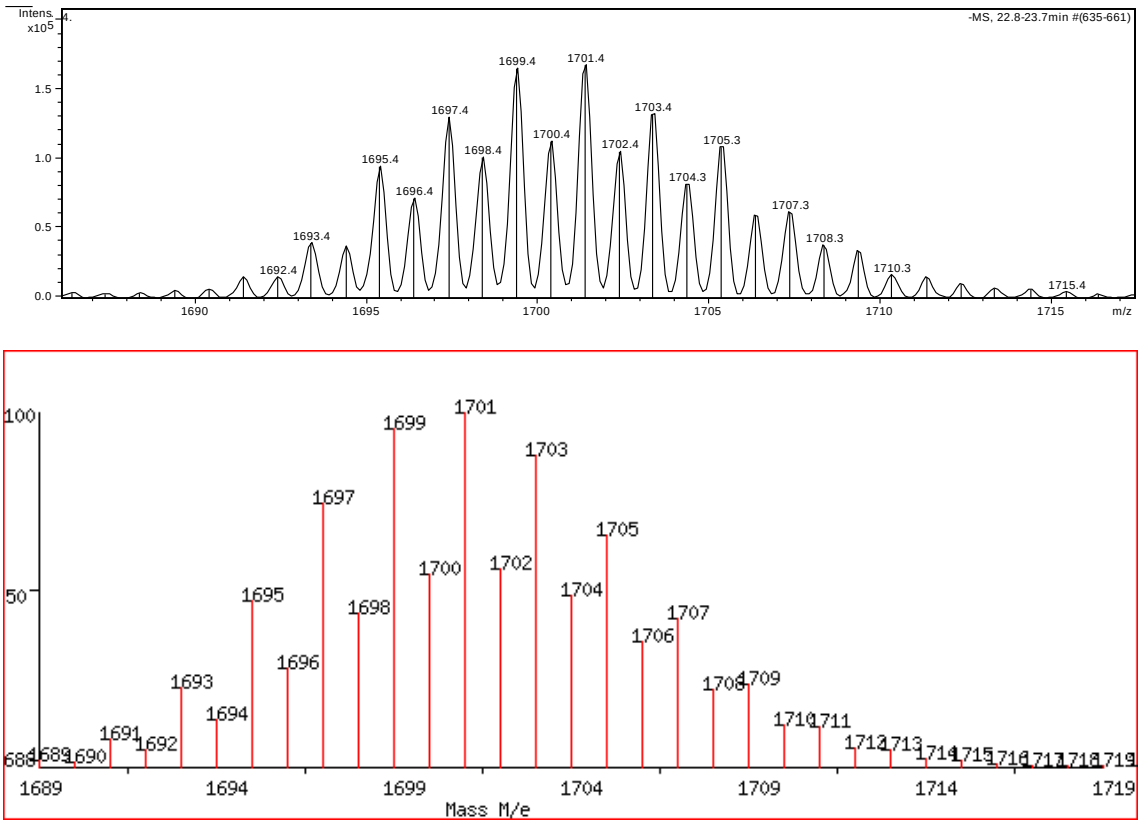

Figure S28. *Experimental (top) and simulated (bottom) LDI-ToF spectra of compound* ***2-R****.*

(c) Longer polyalkyne bridged PTM derivatives

(c.1) Compound 3

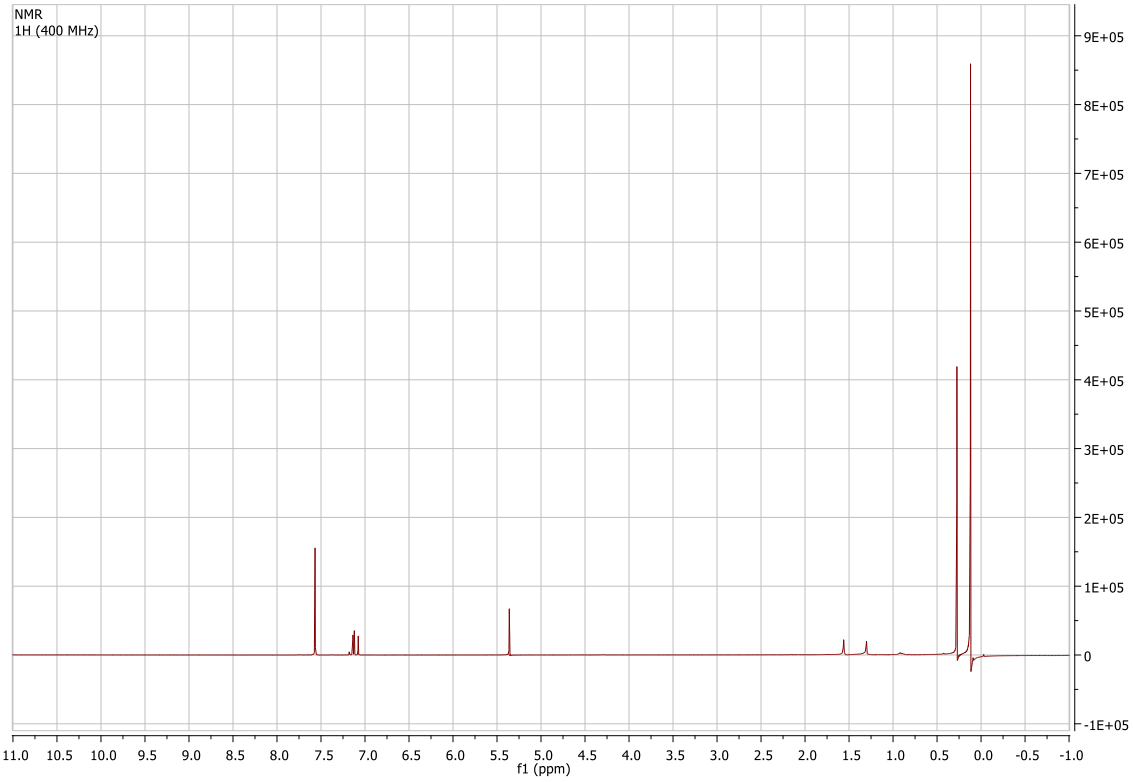

Figure S29. *^{1}H-NMR spectrum of compound **3** in CD_2Cl_2*

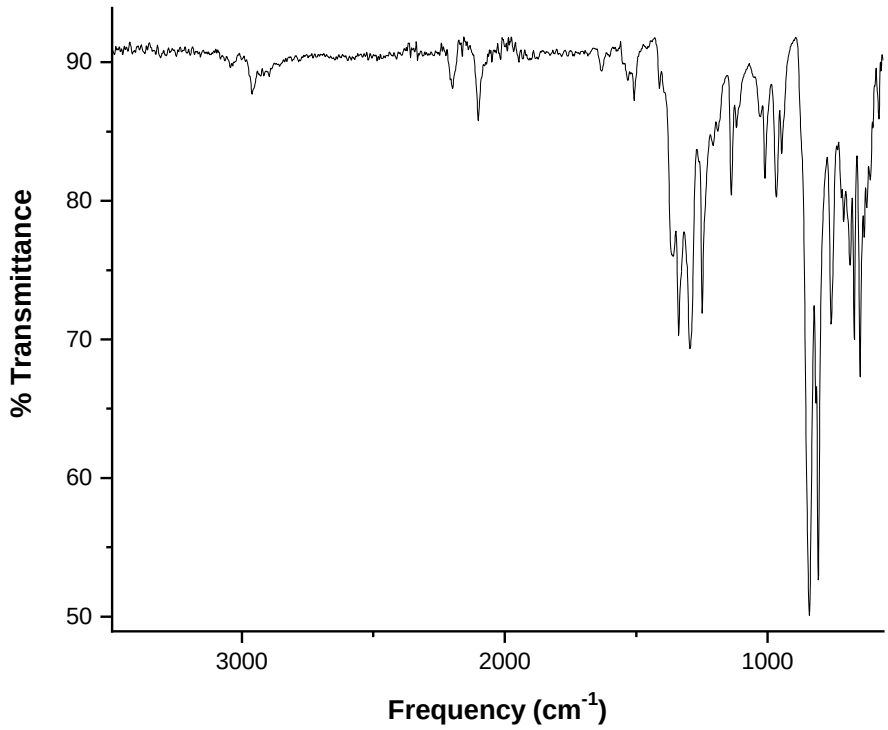

Figure S30. *FT-IR spectrum of compound **3** in powder.*

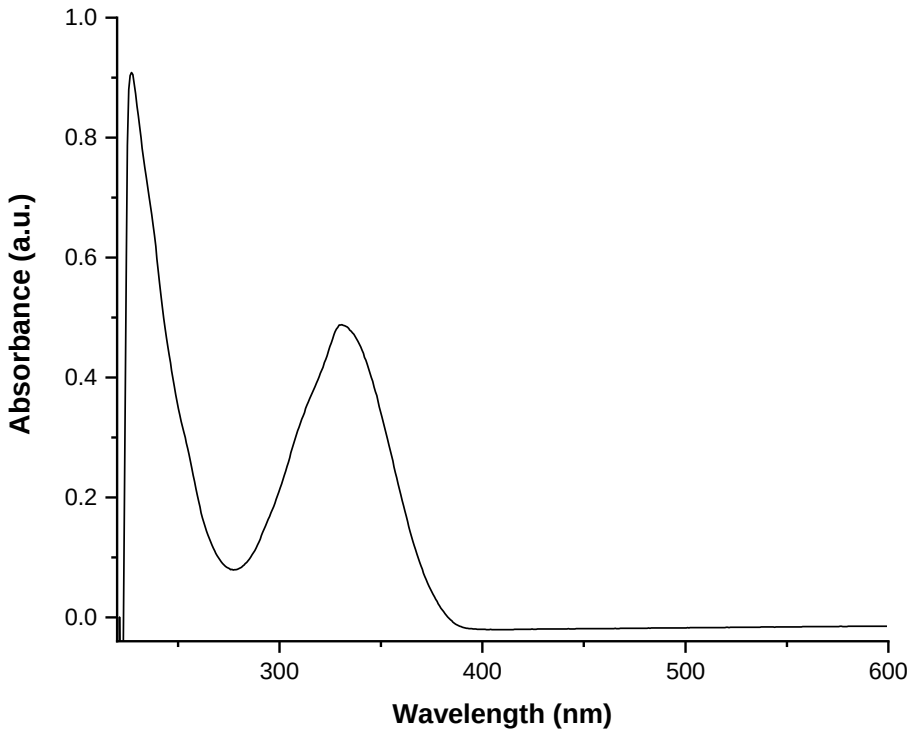

Figure S31. *UV-Vis electronic absorption spectrum of* ***3*** *(9.8 × 10^{-6} M) in THF*

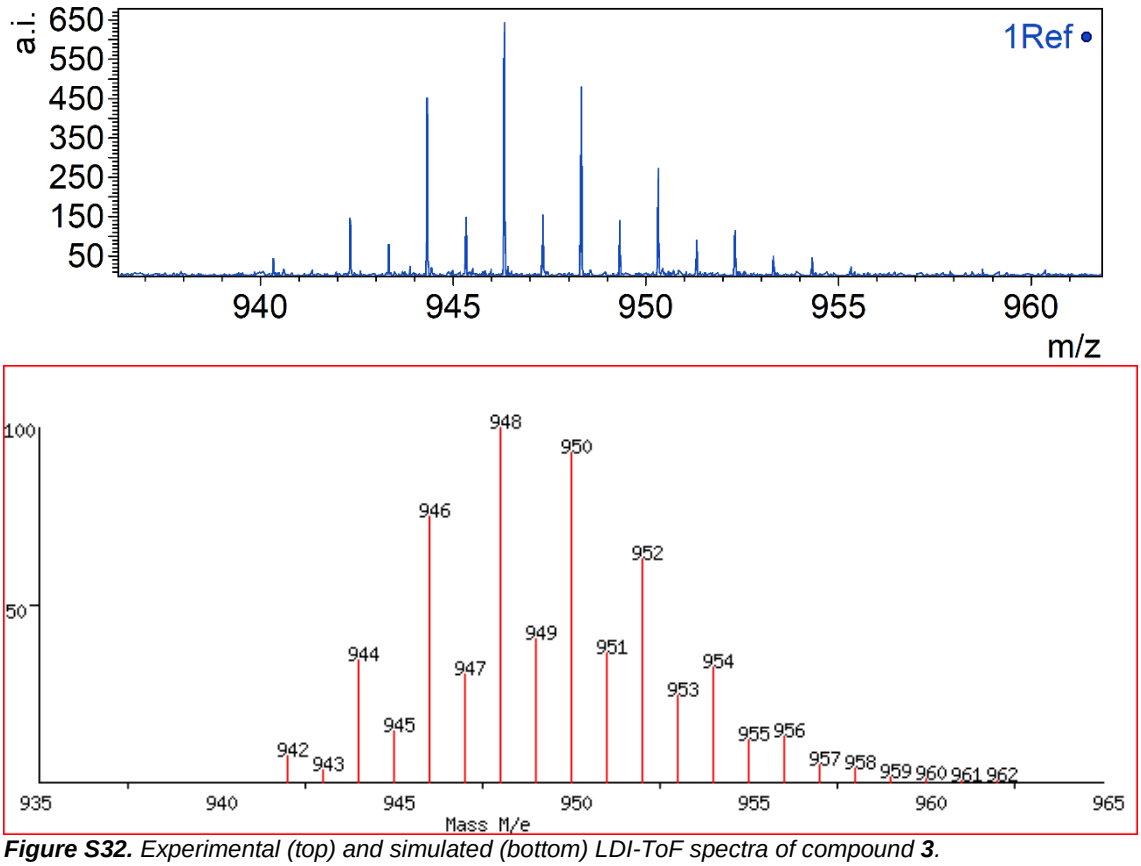

Figure S32. *Experimental (top) and simulated (bottom) LDI-ToF spectra of compound* ***3****.*

(c.2) **Compound 4-H**

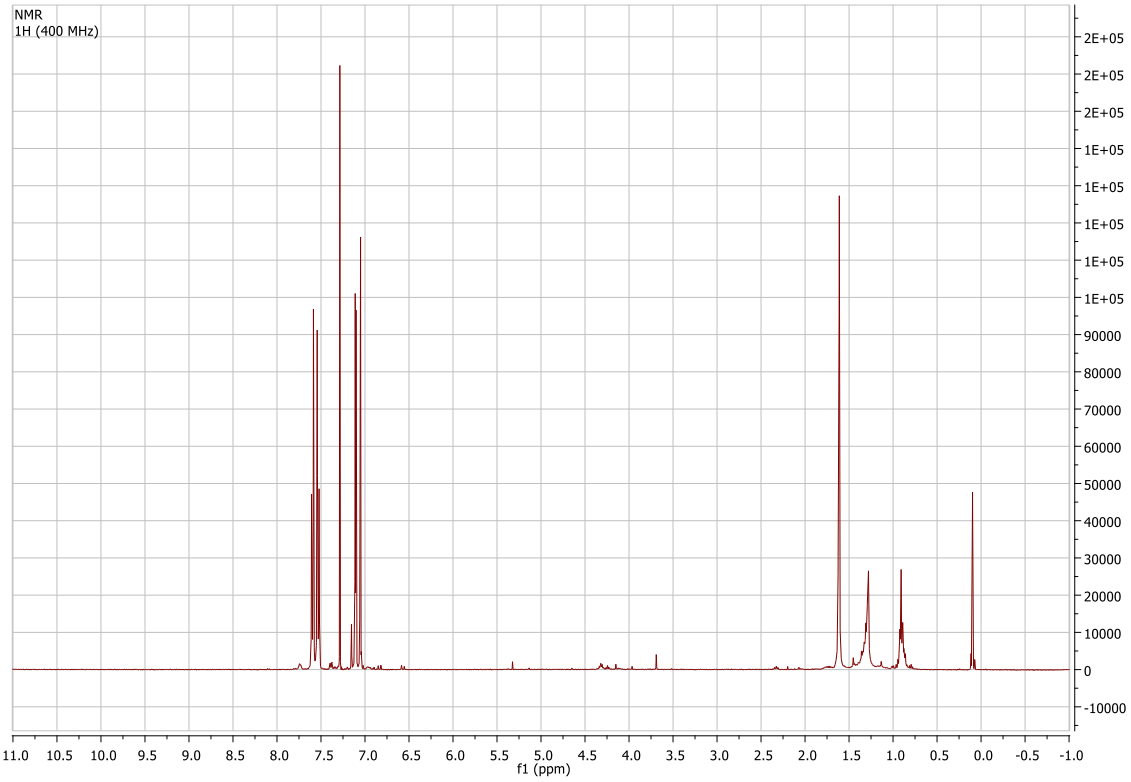

Figure S33. *^{1}H-NMR spectrum of compound* ***4-H*** *in CD_2Cl_2.*

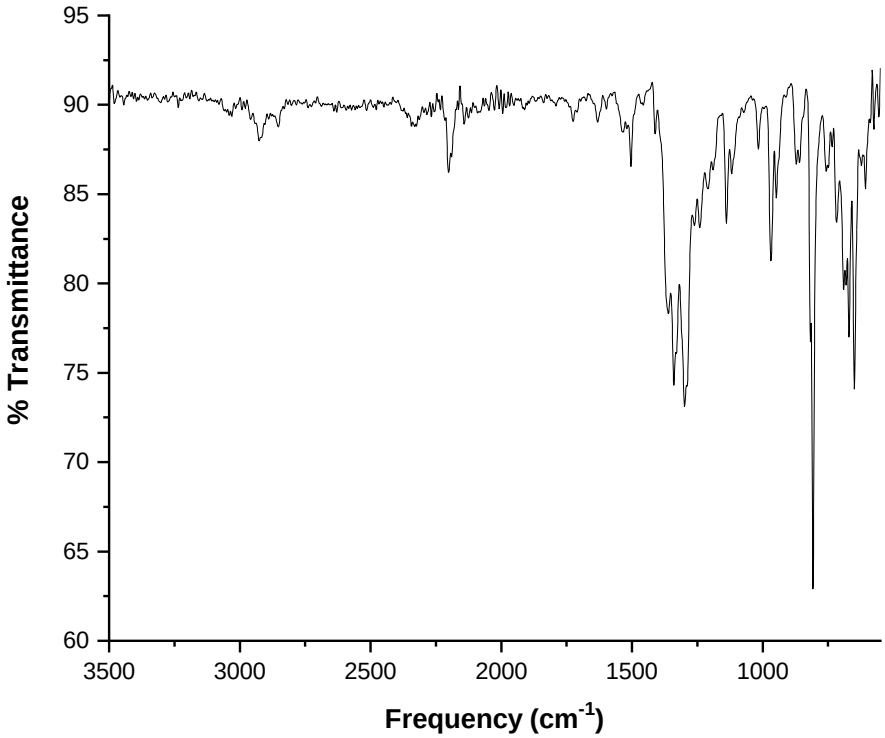

Figure S34. *FT-IR spectrum of compound* ***4-H*** *in powder.*

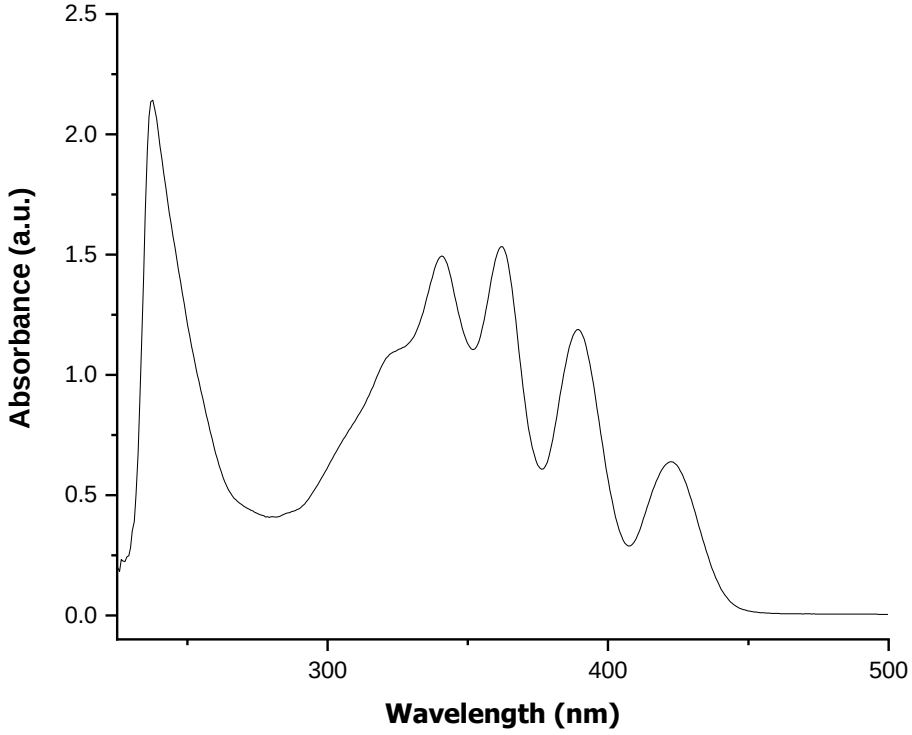

Figure S35. *UV-Vis electronic absorption spectrum of compound* ***4-H*** *(1.3 × 10^{-5} M) in DCM.*

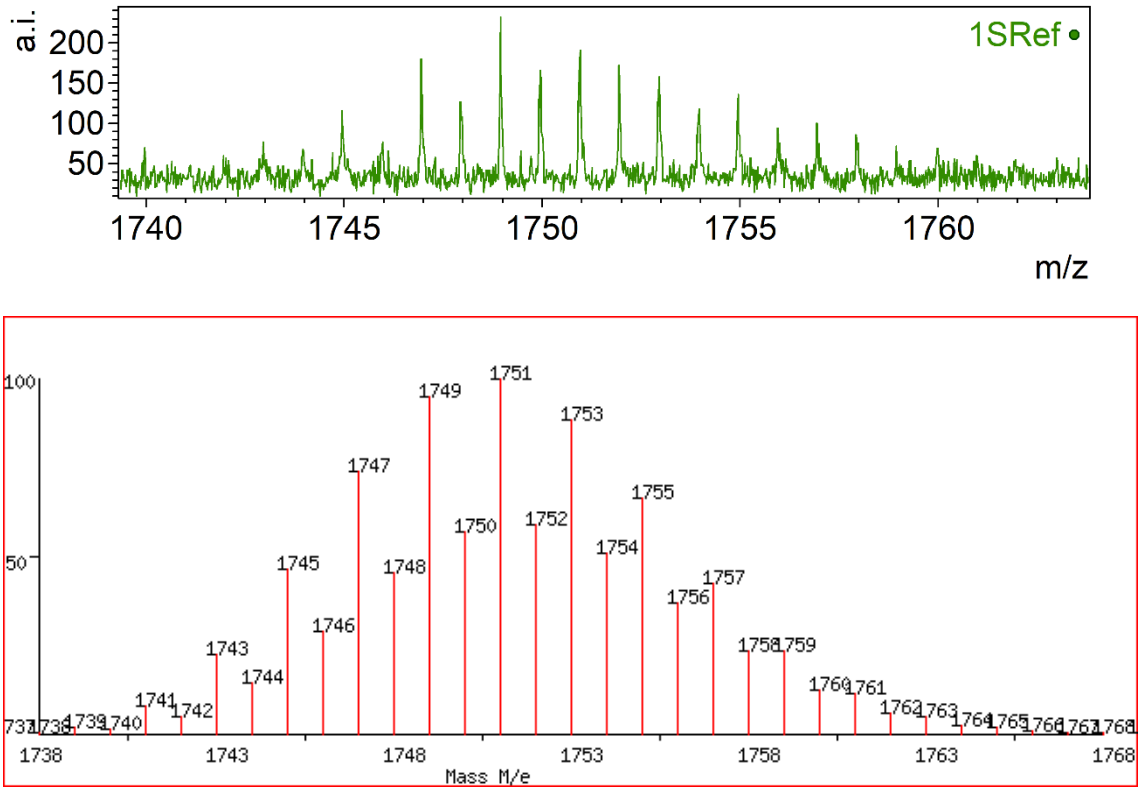

Figure S36. *LDI-ToF spectra of compound* ***4-H*** *experimental (top) and simulated (bottom).*

***(c.3)* Compound 5**

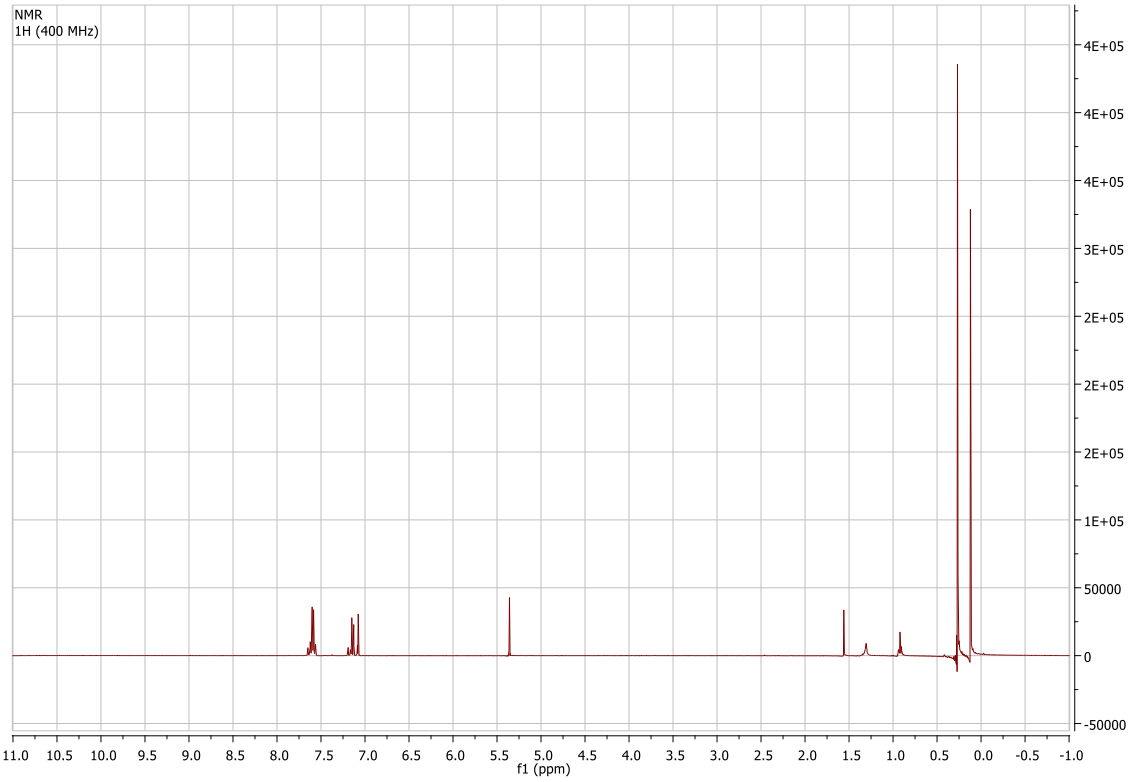

Figure S37. *^{1}H-NMR spectrum of compound* **5** *in CD_2Cl_2.*

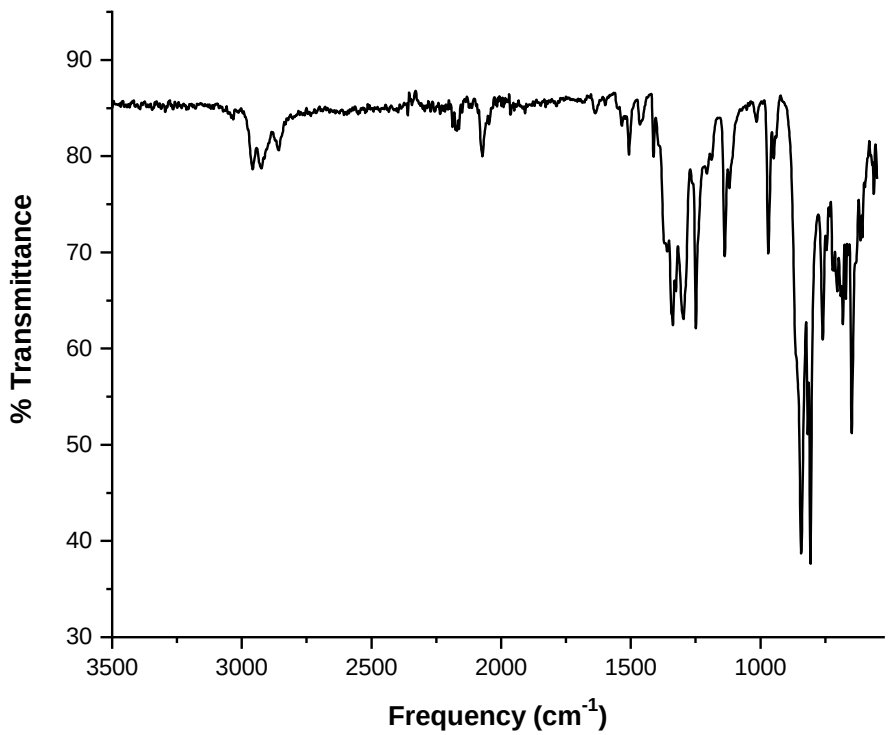

Figure S38. *FT-IR spectrum of compound* **5** *in powder.*

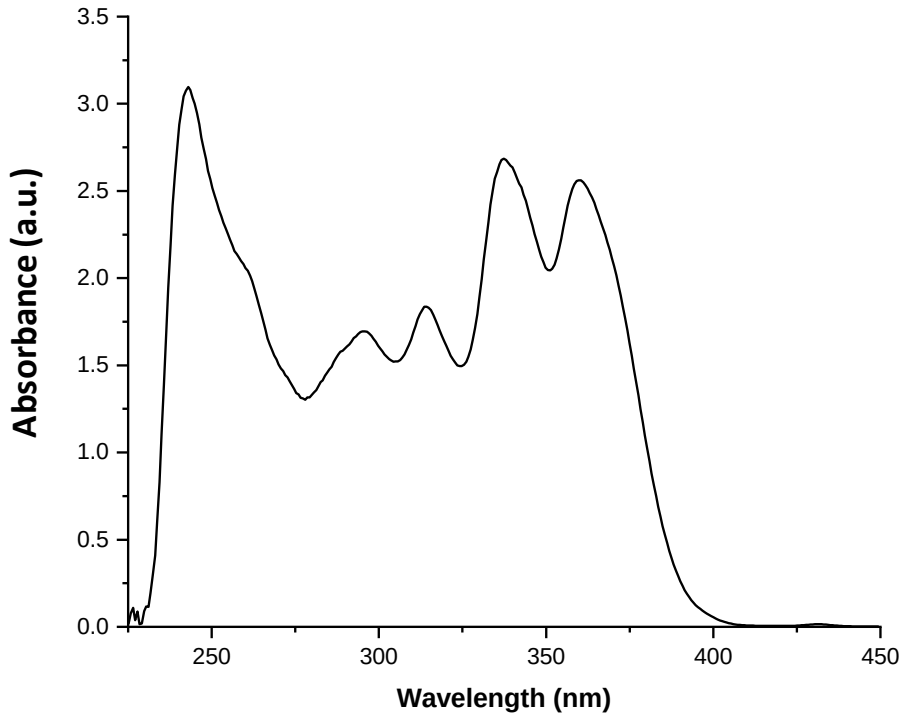

Figure S39. *UV-Vis electronic absorption spectrum of compound* ***5*** *(5.2 × 10^{-5} M) in THF.*

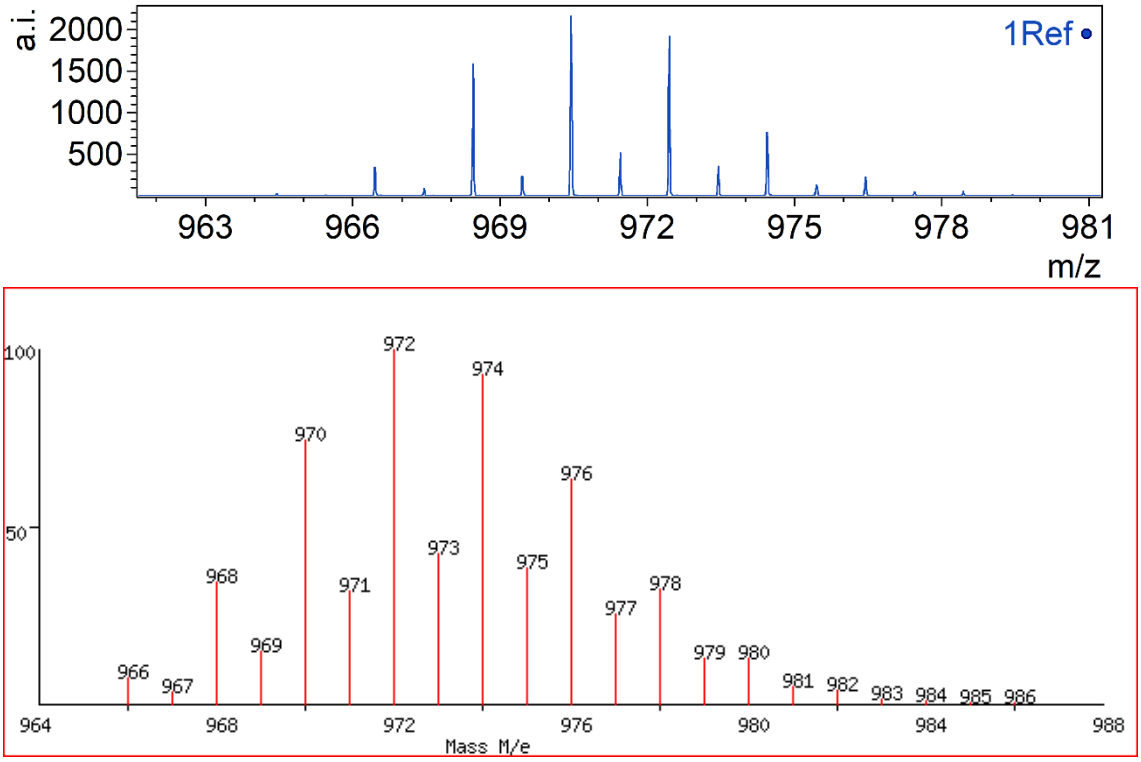

Figure S40. *LDI-ToF spectra of compound* ***5*** *experimental (top) and simulated (bottom).*

(c.4) Compound 6-H

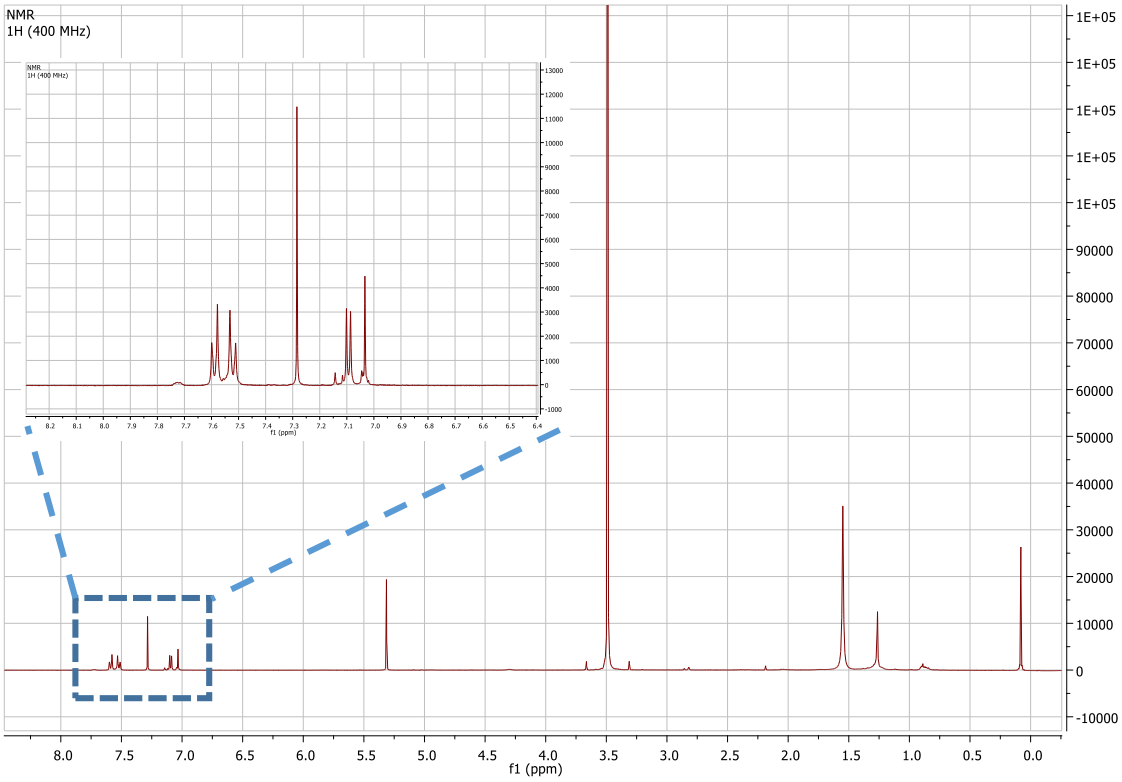

Figure S41. *^{1}H-NMR spectrum of compound **6-H** in $CDCl_3$.*

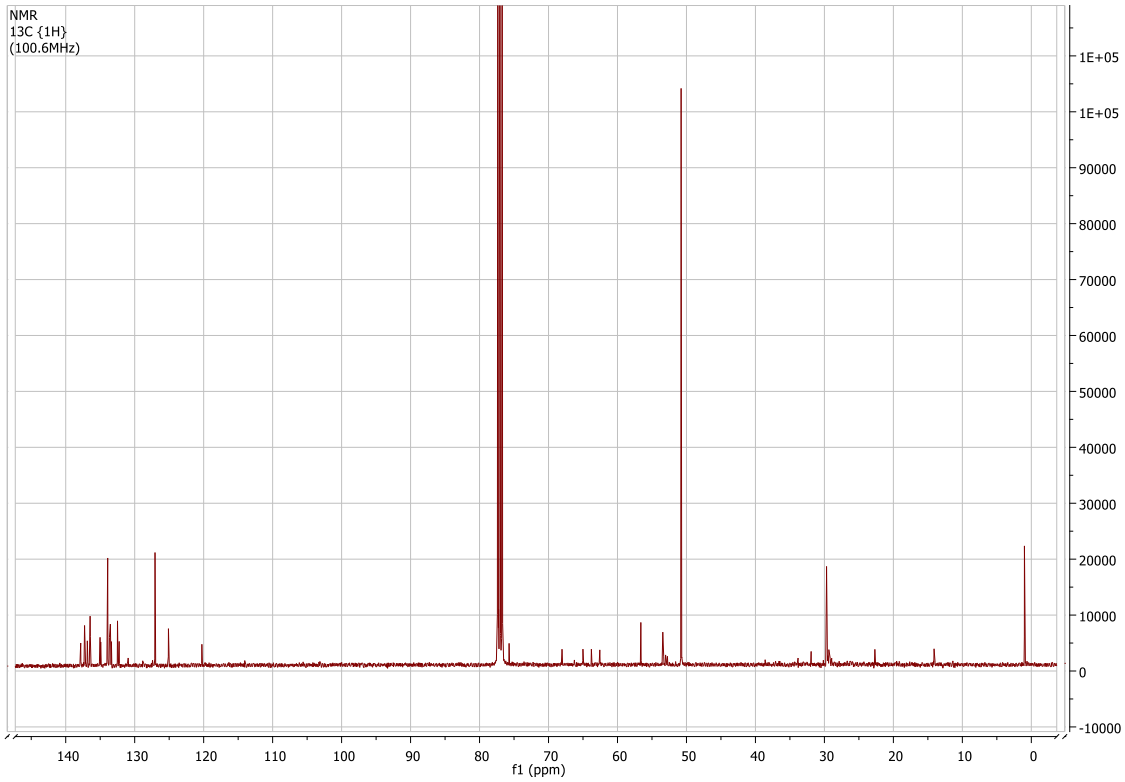

Figure S42. *^{13}C-NMR spectrum of compound **6-H** in $CDCl_3$.*

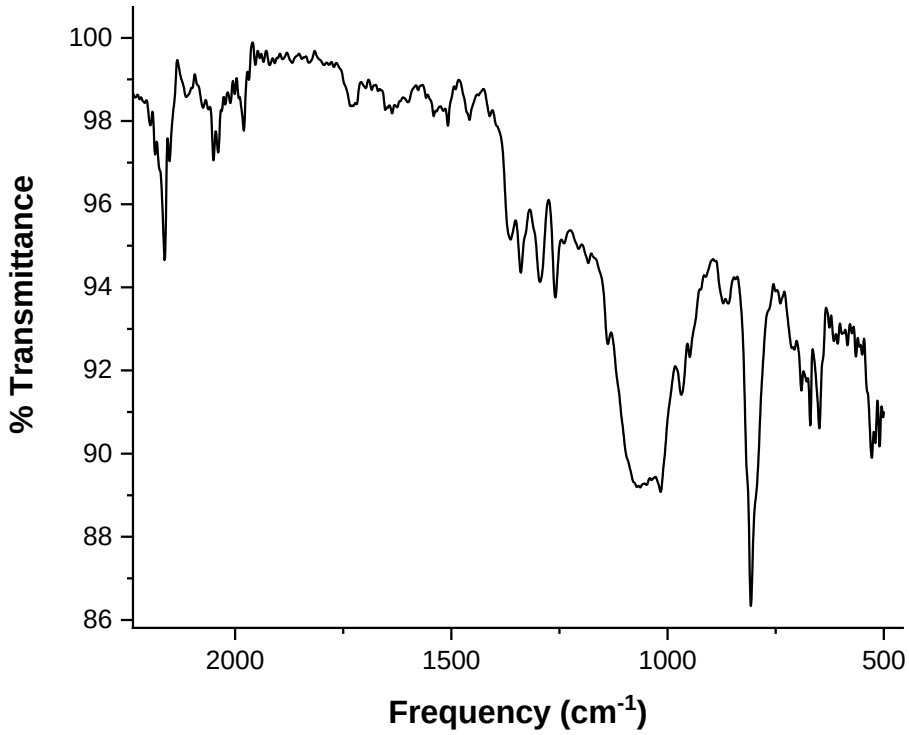

Figure S43. *FT-IR spectrum of compound* ***6-H*** *in powder.*

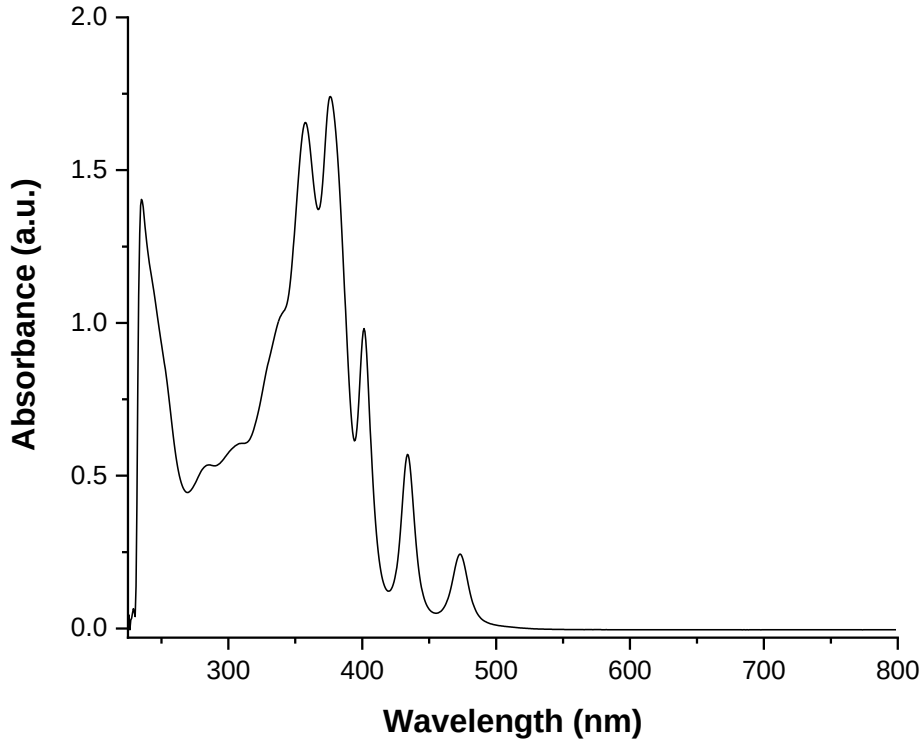

Figure S44. *UV-Vis electronic absorption spectrum of compound* ***6-H*** *(1.3 × 10^{-5} M) in DCM.*

12. References

(1) Bejarano, F.; Olavarria-Contreras, I. J.; Droghetti, A.; Rungger, I.; Rudnev, A.; Gutiérrez, D.; Mas-Torrent, M.; Veciana, J.; van der Zant, H. S. J.; Rovira, C.; *et al.* Robust Organic Radical Molecular Junctions Using Acetylene Terminated Groups for C–Au Bond Formation. *J. Am. Chem. Soc.* **2018,** *140*, 1691–1696.

(2) Dumur, F.; Gautier, N.; Gallego-Planas, N.; Şahin, Y.; Levillain, E.; Mercier, N.; Hudhomme, P.; Masino, M.; Girlando, A.; Lloveras, V.; *et al.* Novel Fused D-A Dyad and A-D-A Triad Incorporating Tetrathiafulvalene and p-Benzoquinone. *J. Org. Chem.* **2004**, *69*, 2164–2177.

(3) Veciana, J.; Riera, J.; Castañer, J.; Ferrer, N. Synthesis and Properties of the 1/1 Complex of 1,4,7,10,13,16-hexaoxacyclooctadecane with Potassium perchlorotriphenylmethide. *J. Org. Chem.* **1985**, *297*, 131–141.

(4) Lewis, F. D.; Bedell, A. M.; Dykstra, R. E.; Elbert, J. E., Gould, I. R.; Farid, S.; Photochemical Generation, Isomerization, and Oxygenation of Stilbene Cation Radicals. *J. Am. Chem. Soc.***1990**, *112*, 8055–8064.

(5) Majima, T.; Tojo, S.; Ishida, A; Takamuku, S. Reactivities of Isomerization, Oxidation, and Dimerization of Radical Cations of Stilbene Derivatives. *J. Phys. Chem.* **1996**, *100,* 13615–13623.

(6) Frisch, M. J. *et al.* Gaussian 16, Revision A.02. Gaussian, Inc., Wallingford CT

(7) Chemcraft - graphical software for visualization of quantum chemistry computations. https://www.chemcraftprog.com/.

(8) Zhao, Y.; Truhlar, D. G. The M06 Suite of Density Functionals for Main Group Thermochemistry, Thermochemical Kinetics, Noncovalent Interactions, Excited States, and Transition Elements: Two New Functionals and Systematic Testing of four M06-class Functionals and 12 Other Function. *Theor. Chem. Acc.* **2008**, *120,* 215–241.

(9) Rassolov, V. A.; Ratner, M. A.; Pople, J. A.; Redfern, P. C.; Curtiss, L. A. 6-31G* basis set for third-row atoms. *J. Comput. Chem.* **2001**, *22,* 976–984.

(10) Ditchfield, R.; Hehre, W. J; Pople, J. A. Self-Consistent Molecular-Orbital Methods. IX. An Extended Gaussian-Type Basis for Molecular-Orbital Studies of Organic Molecules. *J. Chem. Phys.* **1971**, *54,* 724–728.

(11) Grimme, S.; Antony, J.; Ehrlich, S.; Krieg, H. A Consistent and acurate *ab initio* Parametrization of Density Functional Dispersion Correction (DFT-D) for the 94 Elements H-Pu. *J. Chem. Phys.* **2010,** *132,* 154104.

(12) Grimme, S.; Ehrlich, S.; Goerigk, L. Effect of the Damping Function in Dispersion Corrected Density

Functional Theory. *J. Comput. Chem.* **2011**, ***32,*** 1456–1465..

(13) Marenich, A. V.; Cramer, C. J; Truhlar, D. G. Universal Solvation Model Based on Solute Electron Density and on a Continuum Model of the Solvent Defined by the Bulk Dielectric Constant and Atomic Surface Tensions. *J. Phys. Chem. B* **2009,** *113,* 6378–6396.

(14) Grimme, S. Supramolecular Binding Thermodynamics by Dispersion-Corrected Density Functional Theory. *Chem. Eur. J.* **2012**, *18,* 9955–9964.

(15) Casida, M. E.; Jamorski, C.; Casida, K. C.; Salahub, D. R. Molecular Excitation Energies to High-lying Bound States from Time-Dependent Density-Functional Response Theory: Characterization and Correction of the Time-Dependent Local Density Approximation Ionization Threshold. *J. Chem. Phys.* **1998,** *108,* 4439–4449.

(16) Scalmani, G.; Frisch, M. J.; Mennucci, B.; Tomasi, J.; Cammi, R.; Barone V. Geometries and Properties of Excited States in the Gas Phase and in Solution: Theory and Application of a Time-Dependent Density Functional Theory Polarizable Continuum Model. *J. Chem. Phys.* **2006**, *124,* 094107.

(17) Yanai, T.; Tew, D. P.; Handy, N. C. A New Hybrid Exchange–Correlation Functional Using the Coulomb-Attenuating Method (CAM-B3LYP). *Chem. Phys. Lett.* **2004**, *393*, 51–57.